Supporting Information for "Affinity-Selected Bicyclic Peptide G-Quadruplex Ligands Mimic a Protein-like Binding Mechanism"

Kim C. Liu,[†] Konstantin Röder,[†] Clemens Mayer,[†,§] Santosh Adhikari,[†] David J. Wales,[*,†] and Shankar Balasubramanian[*,†,‡,¶]

[†]*Department of Chemistry, University of Cambridge, Lensfield Road, CB2 1EW, Cambridge, UK*

[‡]*Cancer Research UK, Cambridge Institute, Li Ka Shing Centre, Robinson Way, Cambridge, CB2 0RE, UK*

[¶]*School of Clinical Medicine, University of Cambridge, Addenbrooke's Hospital, Hills Road, Cambridge, CB2 0SP, UK*

[§]*Stratingh Institute, University of Groningen, Nijenborgh 4, Groningen, The Netherlands*

E-mail: dw34@cam.ac.uk; sb10031@cam.ac.uk

S1 Supplementary experimental data

S1.1 Phage titers and library complexity across successive selection rounds indicate successful selection

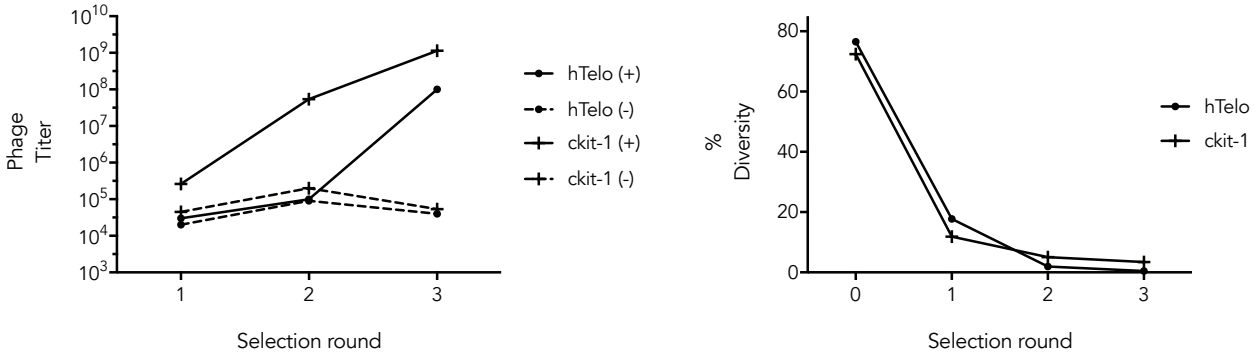

Figure S1: Left: Phage titers (infective phage count) across successive rounds of selection, indicative of number of surviving phages. Increase in phage titers reflects increased G4-binding phenotype within the phage population. Both selections show significant enrichment against no-oligonucleotide negative control. Selection against structurally homogenous ckit-1 shows faster enrichment over structurally heterogenous hTelo. Right: Diversity of phage library (unique peptide count/total peptide count) concomitantly decreases with rounds of selection, as expected for an artificial evolution process.

S1.2 Linear counterparts to bicyclic peptides do not bind G4s

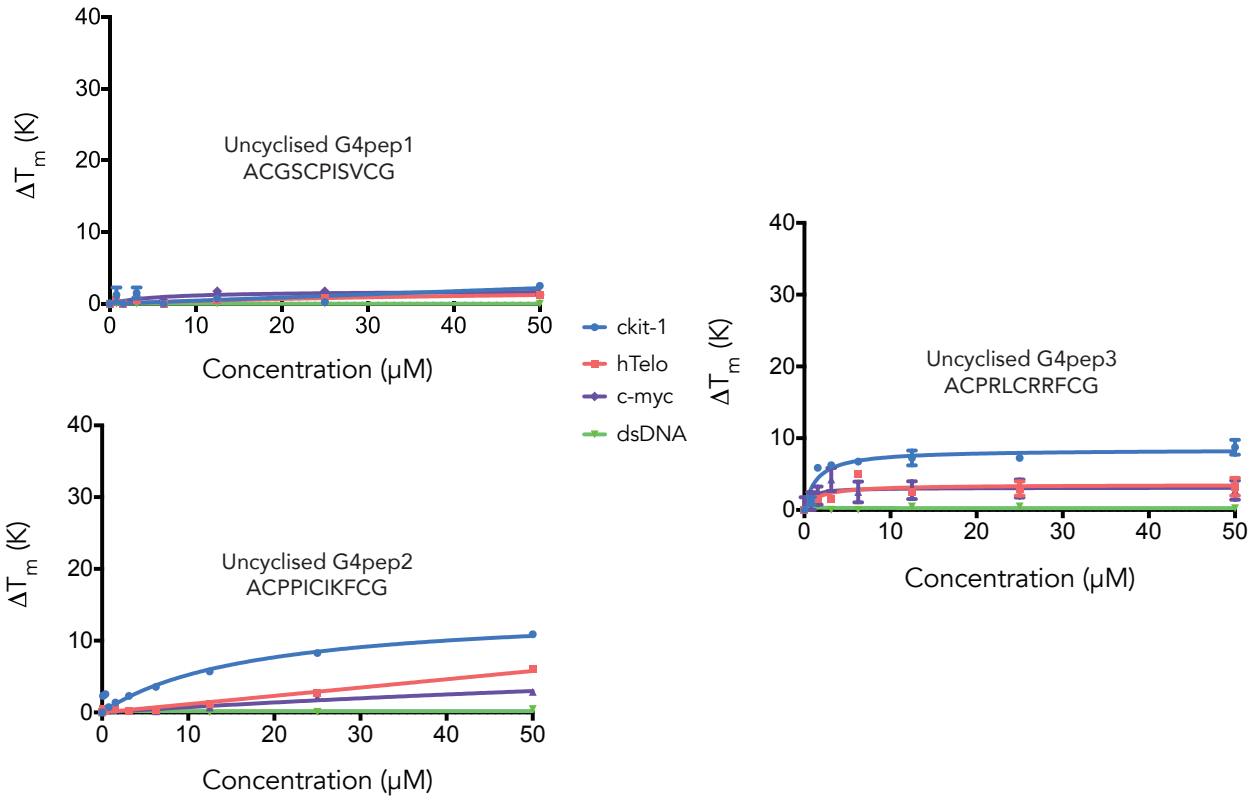

Figure S2: All uncyclised, linear peptides show significantly reduced binding ability, indicating that three-dimensional structure is necessary for G4 recognition.

S1.3 Low-energy structure of b-G4pep2:ckit-1

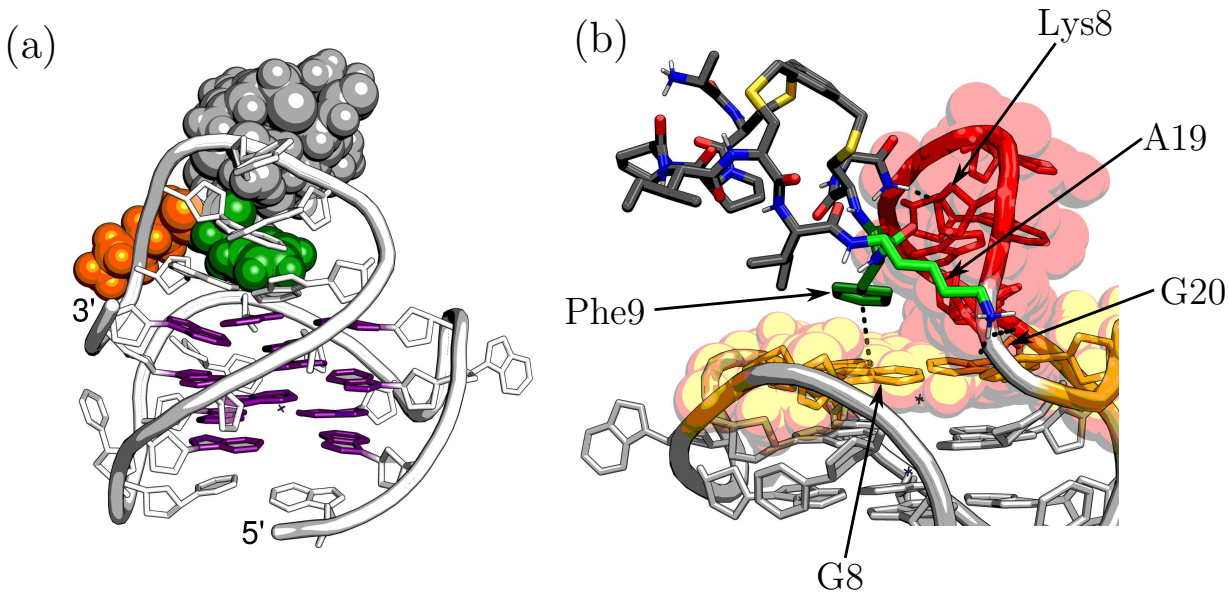

Figure S3: Low-energy structure of b-G4pep2 (b-ACPPICIKFCG):ckit-1 complex. Detail shows Coloumbic interactions between Lys8 and G20 and a $\pi-\pi$ stacking interaction between Phe9 and the $3'$-tetrad.

S1.4 Complete biophysical data

T_m stabilisation by FRET

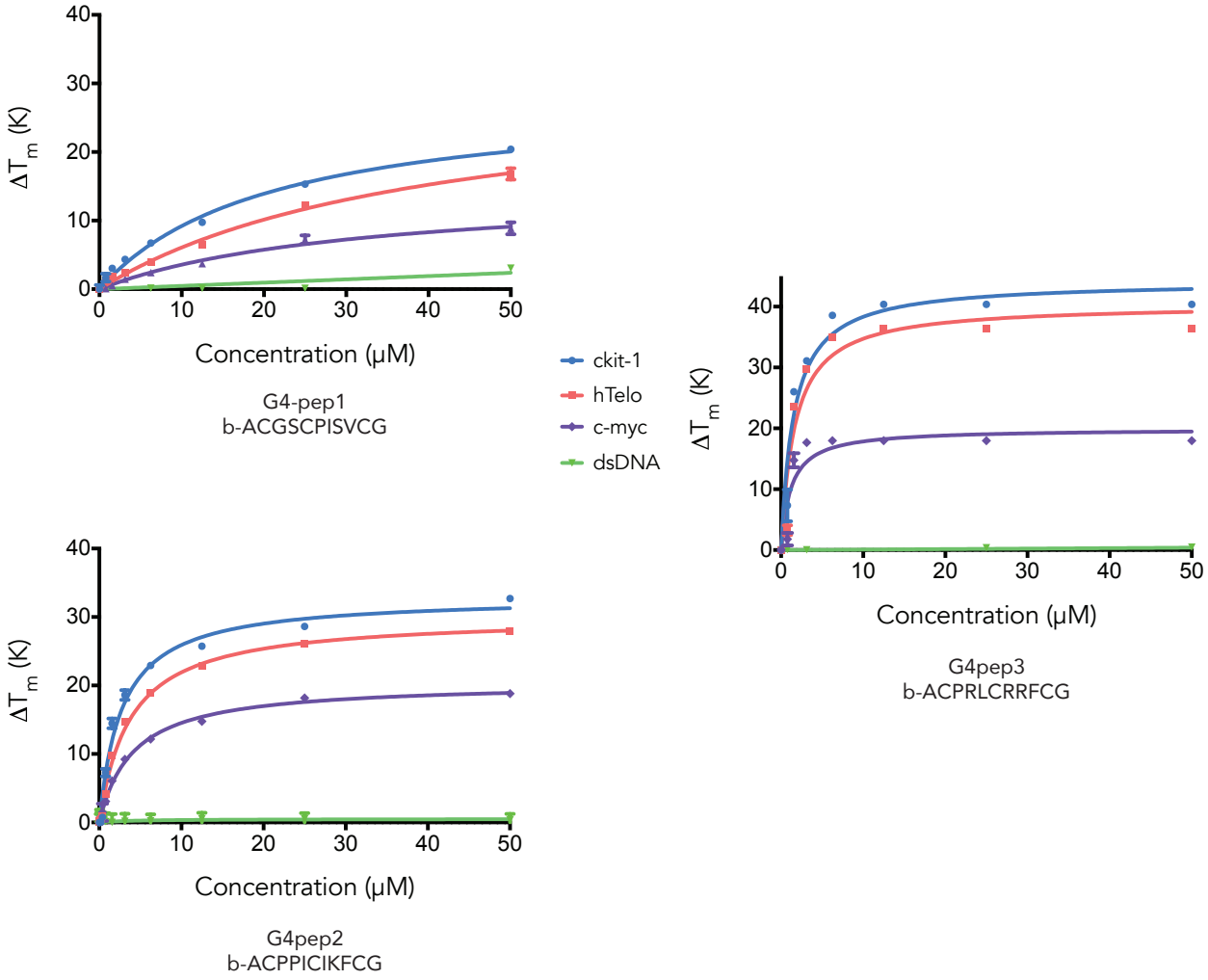

Figure S4: FRET melting curves for b-G4pep1, b-G4pep2 and b-G4pep3 with panel of dual-labelled G4 oligonucleotides originating from the human genome: ckit-1, hTelo, c-myc and a short double-stranded DNA.

FRET competition assay

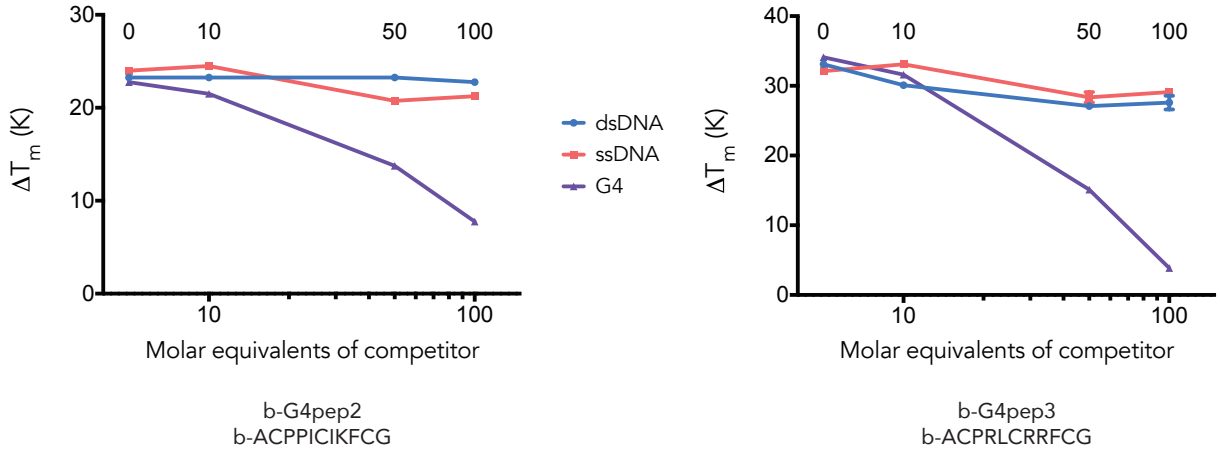

b-G4pep2
b-ACPPICIKFCG

b-G4pep3
b-ACPRLCRRFCG

Figure S5: FRET melting at 5 μM for b-G4pep2 and b-G4pep3 was carried out in the presence of increasing amounts of unlabelled dsDNA, ssDNA and G4 (ckit-1) competitor. As expected, the unlabelled G4 significantly reduces observed ΔT_m, but high specificity is seen against dsDNA and ssDNA in both bicyclic peptides.

Fluorescence quench equilibrium binding assay

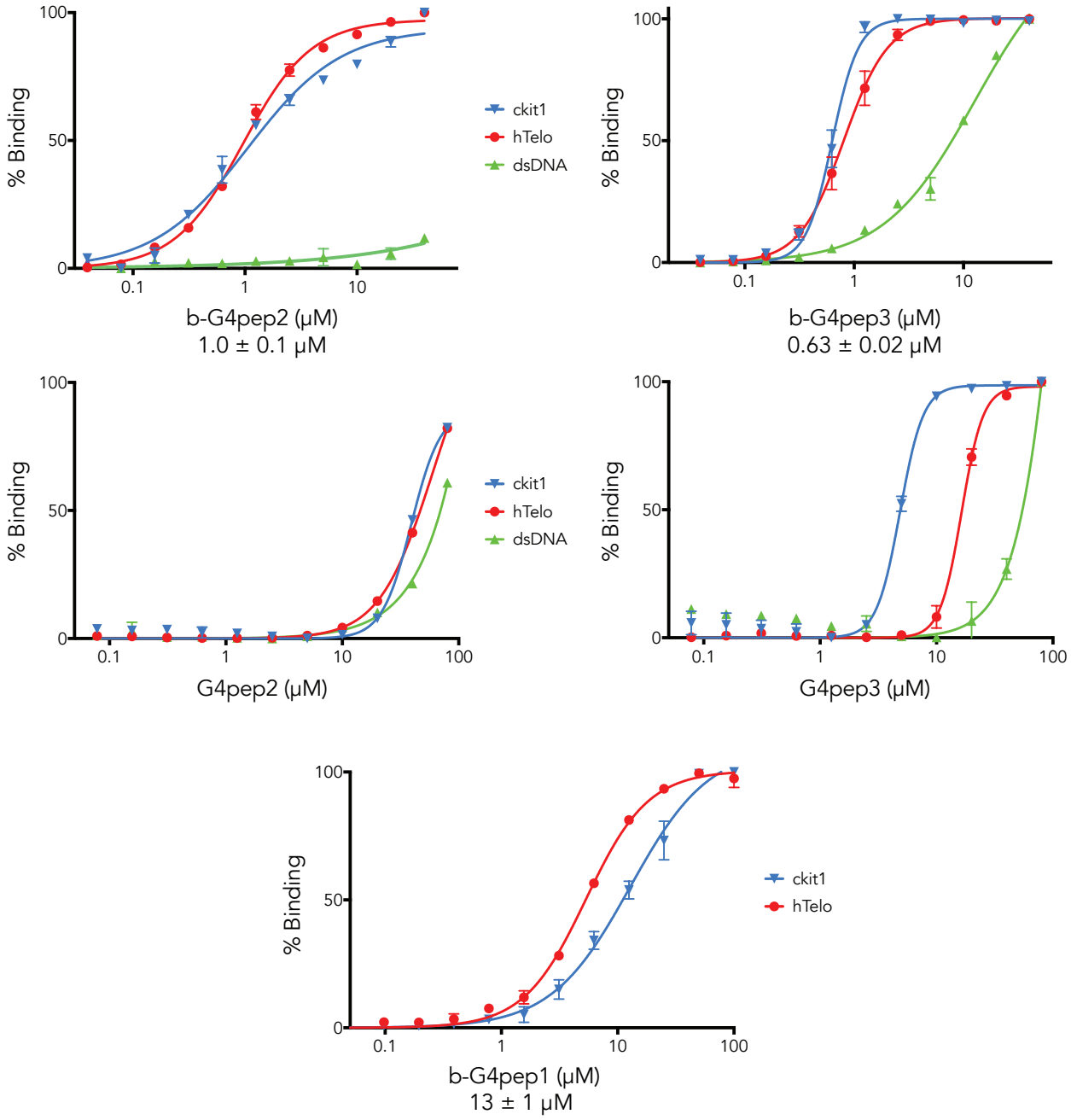

Figure S6: Fluorescence quench equilibrium binding assays generate apparent K_ds for bicyclic and linear peptide-G4 complexes. K_ds for ckit-1 are quoted.

S1.5 Circular dichroism spectra of bicyclic peptide G4 ligands

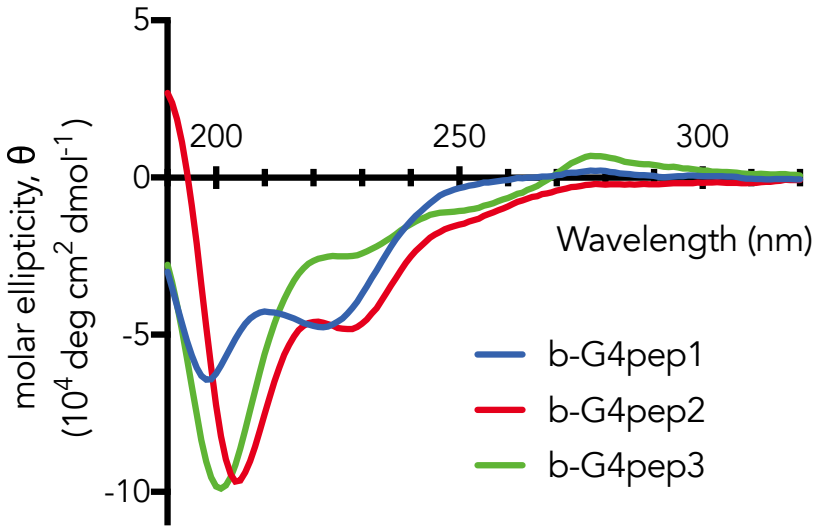

Figure S7: Circular dichroism spectra of three bicyclic peptide G4 ligands (50 μM in water).

S1.6 Starting library characterisation

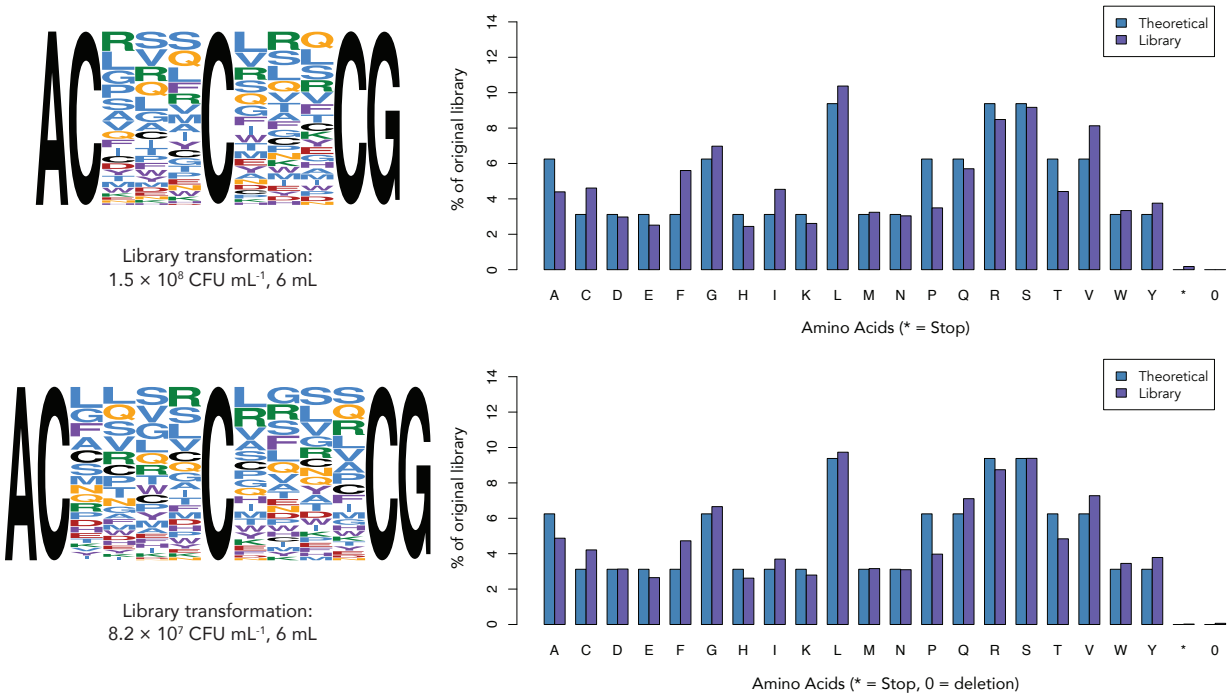

Figure S8: Characterisation of 3×3 (top) and 4×4 (bottom) phage display libraries. For each library, SeqLogos demonstrate even amino acid distribution at each variable position. Amino acid residue colours: blue – hydrophobic, purple – aromatic, yellow – amide, green – basic, red – acidic. Library transformation estimated by counting colony forming units (CFU) after transformation of phage display library into *E. coli*. Bar chart compares total amino acid proportions with expected proportions calculated using TG1 *E. coli* NNK codons.

S1.7 Tabulated amino acid enrichment for 3×3 ckit-1 selection

	3	4	5	7	8	9	
D	0.00	0.22	0.01	1.08	0.41	0.01	D
E	0.00	0.19	0.01	1.11	2.05	0.00	E
K	0.01	1.98	0.15	2.05	9.50	0.01	K
R	0.11	2.28	0.06	1.36	4.54	0.01	R
H	0.01	0.33	0.02	0.34	0.77	0.05	H
F	0.00	0.53	5.87	1.24	0.12	9.13	F
W	0.03	0.19	0.34	0.36	0.03	9.95	W
Y	0.00	1.54	1.19	0.49	0.21	4.78	Y
N	0.00	0.77	0.01	3.05	1.42	0.00	N
Q	0.01	1.75	0.01	2.09	2.36	0.03	Q
A	0.01	2.02	0.01	0.87	1.53	0.00	A
C	0.00	0.02	0.01	0.02	0.01	0.08	C
G	0.00	0.60	0.02	1.22	0.07	0.00	G
I	0.00	2.89	3.87	2.14	0.07	0.07	I
L	0.01	0.88	4.01	0.55	0.26	0.12	L
M	0.00	0.33	0.33	0.60	0.12	0.00	M
P	26.65	2.42	0.01	0.04	0.40	0.00	P
S	0.01	0.87	0.02	0.99	0.64	0.01	S
T	0.03	0.21	0.04	2.01	0.40	0.00	T
V	0.00	1.00	1.61	1.05	0.11	0.01	V
*	0.00	0.01	0.19	0.01	0.00	1.28	*

Figure S9: Amino acid enrichment at each variable position for the 3×3 ckit-1 selection, calculated by $P_{\text{after}}/P_{\text{before}}$, the amino acid proportion at each position after and before selection. Highest enrichments are shown in green. The SeqLogo after selection is shown again for reference (represents P_{after}).

S1.8 Bicyclic peptides identified by phage display affinity selection against G4s

4×4, hTelo

Peptide sequence	% repr.
AC--GSCPISVCG	84.53
ACPWNICHQNWCG	3.59
AC--GTCPRGYCG	1.81
ACQVQHCYRGRCG	1.49
ACPWSVCRESWCG	0.84
ACKLKWCEQKYCG	0.61
AC--GSCPMLWCG	0.57
ACNWRVCQKEWCG	0.45
ACGPRWCQIRYCG	0.43
ACRHIFCYKGQCG	0.42

3×3, ckit-1

Peptide sequence	% repr.
ACPPICIKFCG	6.16
ACPIFCGRWCG	5.94
ACPAFCTRFCG	4.15
ACPRLCVRYCG	3.18
ACPYICQKFCG	3.10
ACPQLCFRFCG	2.87
ACPALCFRFCG	2.78
ACPILCREFCG	2.32
ACPRVCDRWCG	1.91
ACPGFCKQWCG	1.87

Figure S10: Enriched peptide sequences in final rounds of selection against hTelo and ckit-1 (first 10), with respective percentage representation in each pool. '–' represents deleted amino acids.

S1.9 Bicyclic peptide characterisation

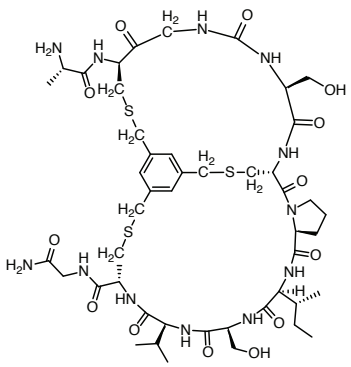

b-G4pep1: b-ACGSCPISVCG, $C_{47}H_{73}N_{12}O_{13}S_3$

$[M+H]^+$ = 1109.4577, found: 1109.4555 (-1.98 ppm)

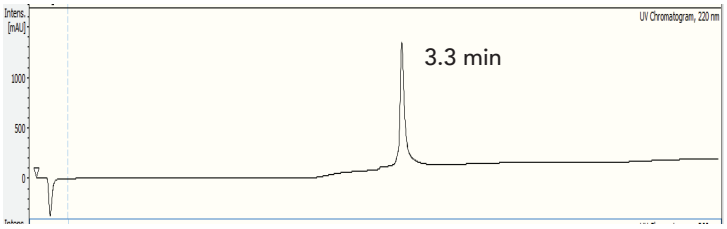

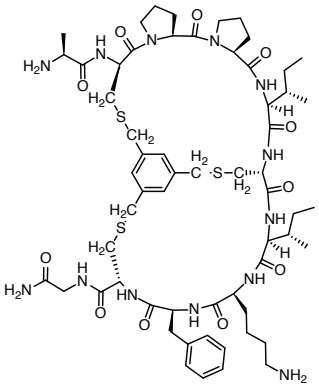

b-G4pep2: b-ACPPICIKFCG, $C_{60}H_{90}N_{13}O_{11}S_3$

$[M+H]^+$ = 1264.6039, found: 1264.6035 (-0.4 ppm)

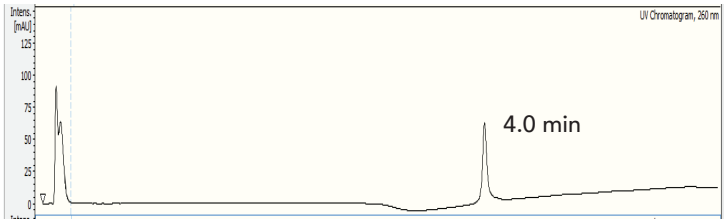

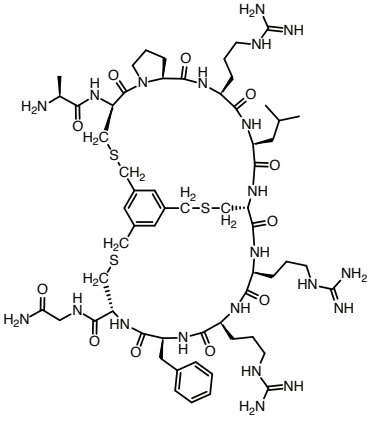

b-G4pep3: b-ACPRLCRRFCG, $C_{61}H_{96}N_{21}O_{11}S_3$

$[M+H]^+$ = 1394.6760, found: 1394.6769 (+0.6 ppm)
$[M+2H]^+$ = 697.8414, found: 697.8416
$[M+3H]^+$ = 697.5633, found: 697.5630

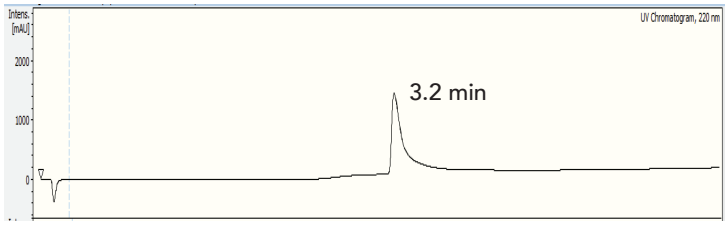

Figure S11: Bicyclic peptides characterised by HRMS and UHPLC at 220 or 260 nm

S1.10 Other bicyclic peptide G4 ligands

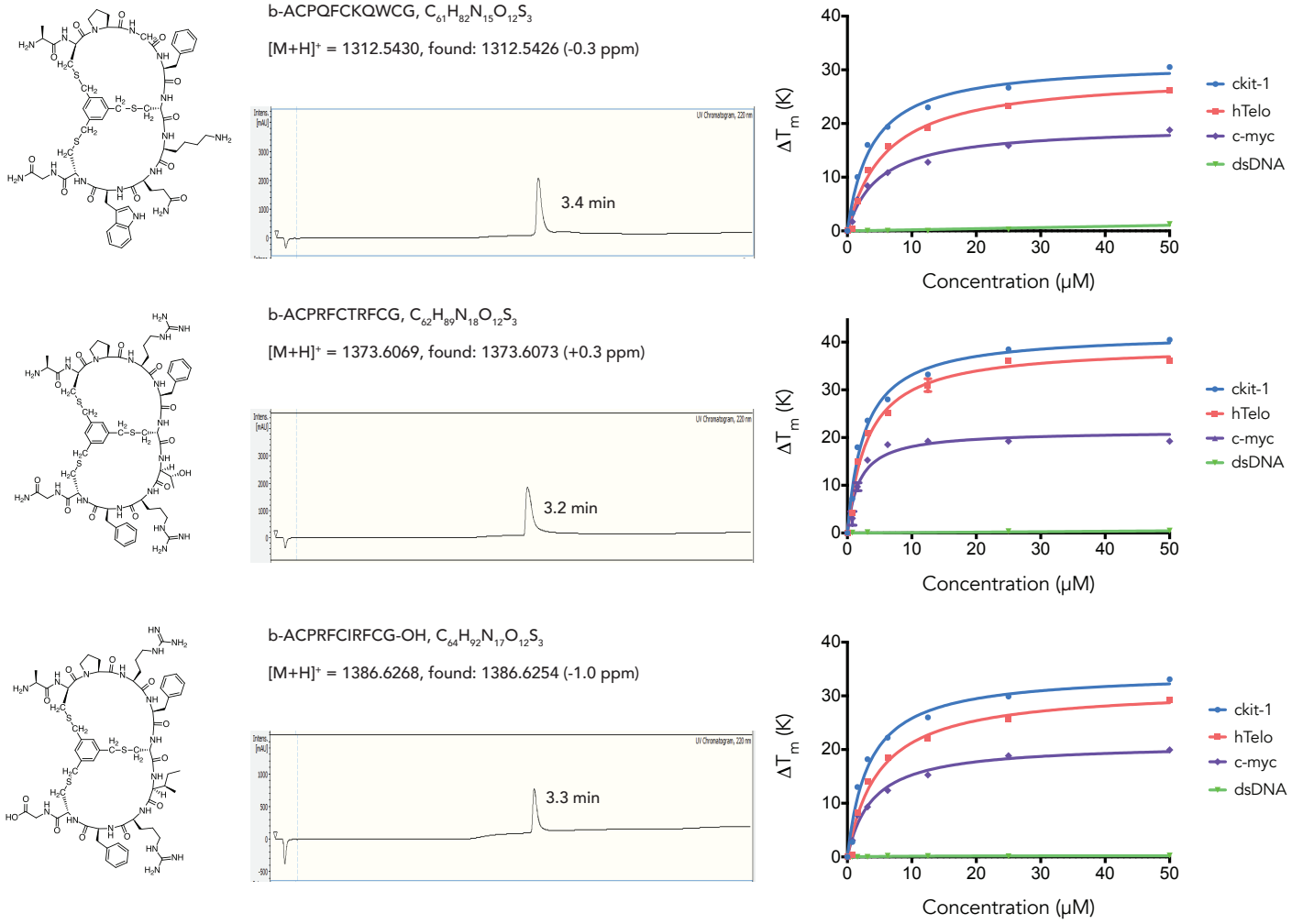

Figure S12: Other bicyclic peptide G4 ligands including synthetic characterisation; G4-binding characterised by FRET melting. These bicyclic peptides follow the SeqLogo motif from Fig. 2b and show comparable G4-binding ability to b-G4pep2.

S2 Characterisation of bicyclic peptides from simulation

For the analysis of the secondary structure of the peptides we considered all minima in the potential energy landscapes to gain an overview of the generic features the structures share. For the displayed structures, we only focus on the lowest energy structures. However, for these rigid peptides the lowest minima are representative, and insight can be gained from a comparison between structures. In Fig. S13 to S16, we illustrate the individual peptides, highlighting a number of features. The linker is shown in orange, the N and C terminal groups in blue and red, respectively, and the positively charged residues are coloured green. None of the peptides contains a negatively charged amino acid. In Table S1, all sequences are shown, with the naming used in our analysis.

Table S1: Overview of the sequences used in the simulations. Seq4 and Seq5 constitute the additional good binders from experiment. Seq7 and Seq8 are sequences lost after the first round of selection. The parts of the sequence in green indicate common sub-sequences, with red highlighting a key difference for b-G4pep1. In early stages of the work, we considered another sequence, Seq6, but decided not to pursue it; hence the labelling of the sequences.

	1	2	3	4	5	6	7	8	9	10	11		Binding simulations?
b-G4pep1	A	C	G	S	C	P	I	S	V	C	G	NH_2	Yes
b-G4pep2	A	C	P	P	I	C	I	K	F	C	G	NH_2	Yes
b-G4pep3	A	C	P	R	L	C	R	R	F	C	G	NH_2	Yes
Seq4	A	C	P	G	F	C	K	Q	W	C	G	NH_2	Yes
Seq5	A	C	P	W	F	C	F	R	W	C	G	NH_2	Yes
Seq7	A	C	M	F	G	C	M	G	P	C	G	NH_2	No
Seq8	A	C	R	W	W	C	L	Q	W	C	G	NH_2	No

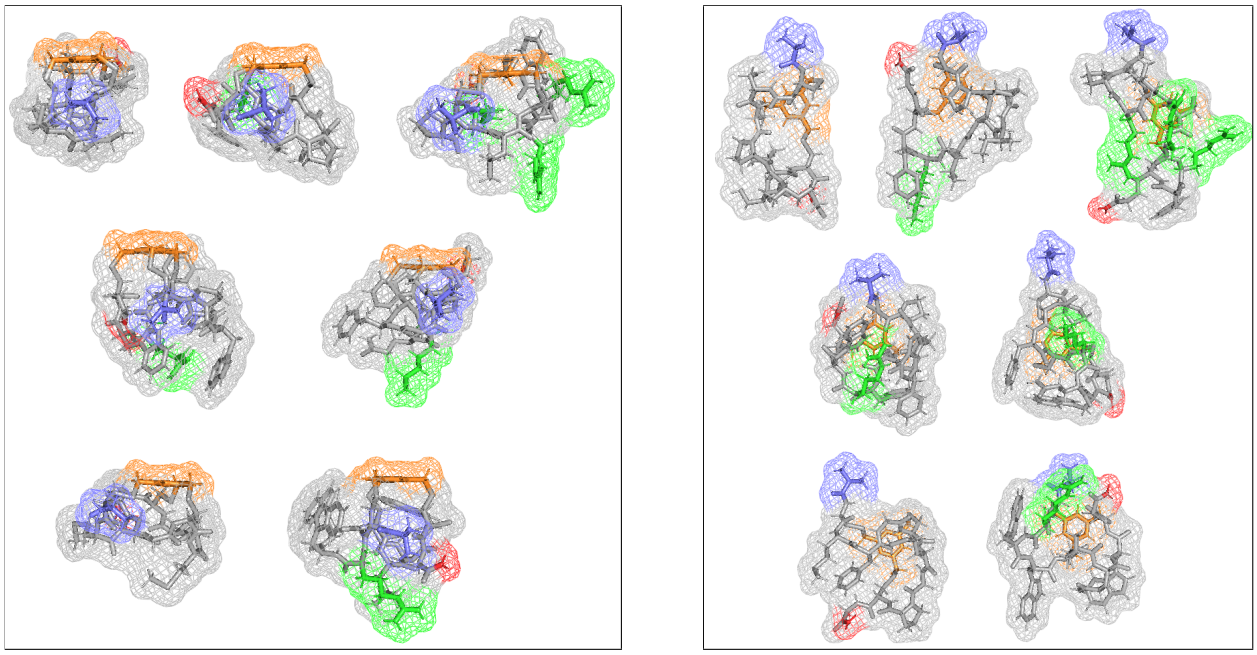

Figure S13: Overview and structural comparison for all bicyclic peptides. Two view points are presented for each structure: the panel on the left has the benzene of the linker horizontally on top and the N-terminus pointing up, and the one on the right has the linker parallel to the page pointing inwards, with the N-terminus pointing up. For each panel from top left to bottom right the sequences are b-G4pep1, b-G4pep2, b-G4pep3, Seq4, Seq5, Seq7 and Seq8.

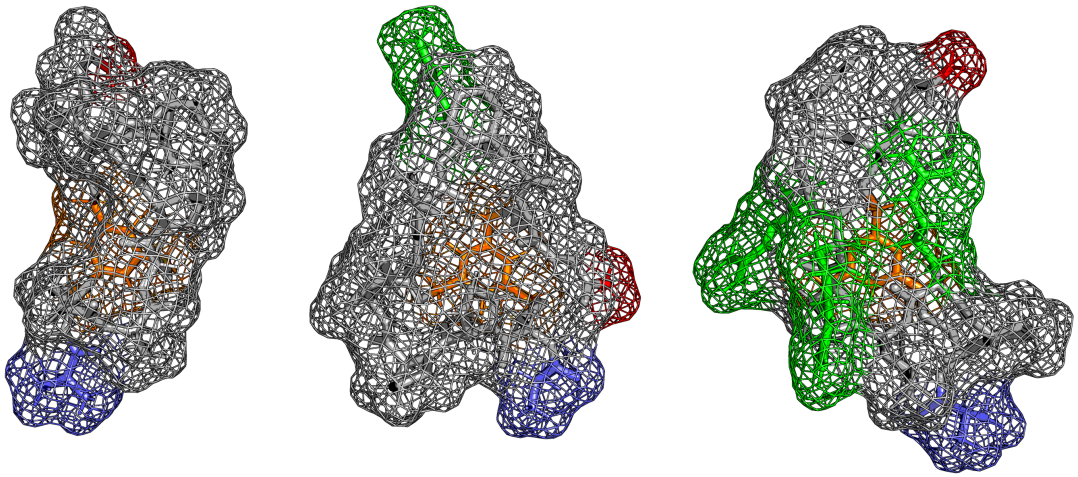

Figure S14: Lowest energy structures for b-G4pep1 to b-G4pep3, illustrating the side opposite the linker (same orientation as in the right hand panel in Fig. S13). The belt-like arrangement for the positive charges in b-G4pep3 is highlighted in green

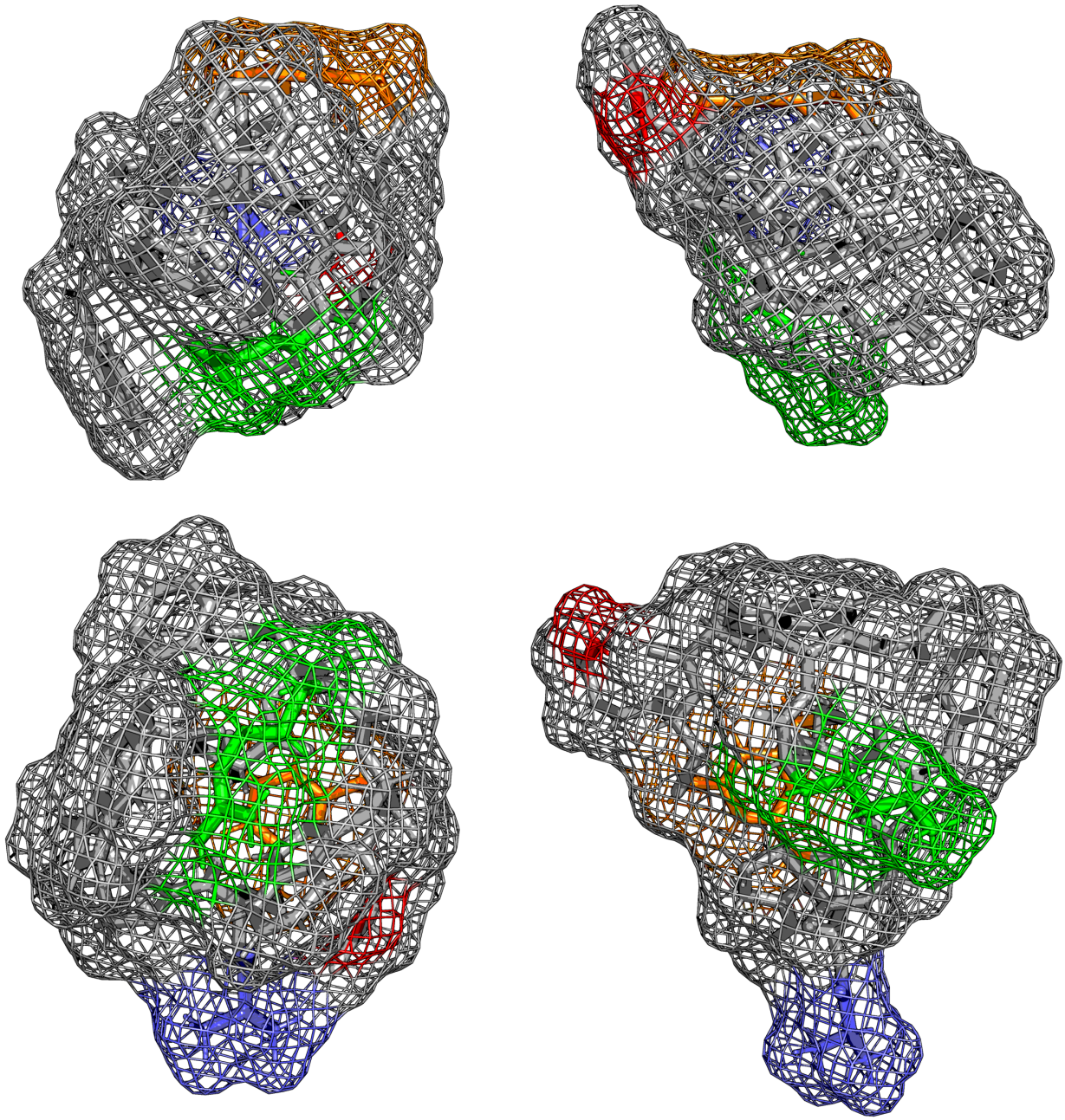

Figure S15: Lowest energy structures for Seq4 (left) and Seq5 (right), viewed from the side (top), and from opposite the linker (bottom). The structures are more spherical than for the best binder (b-G4pep3).

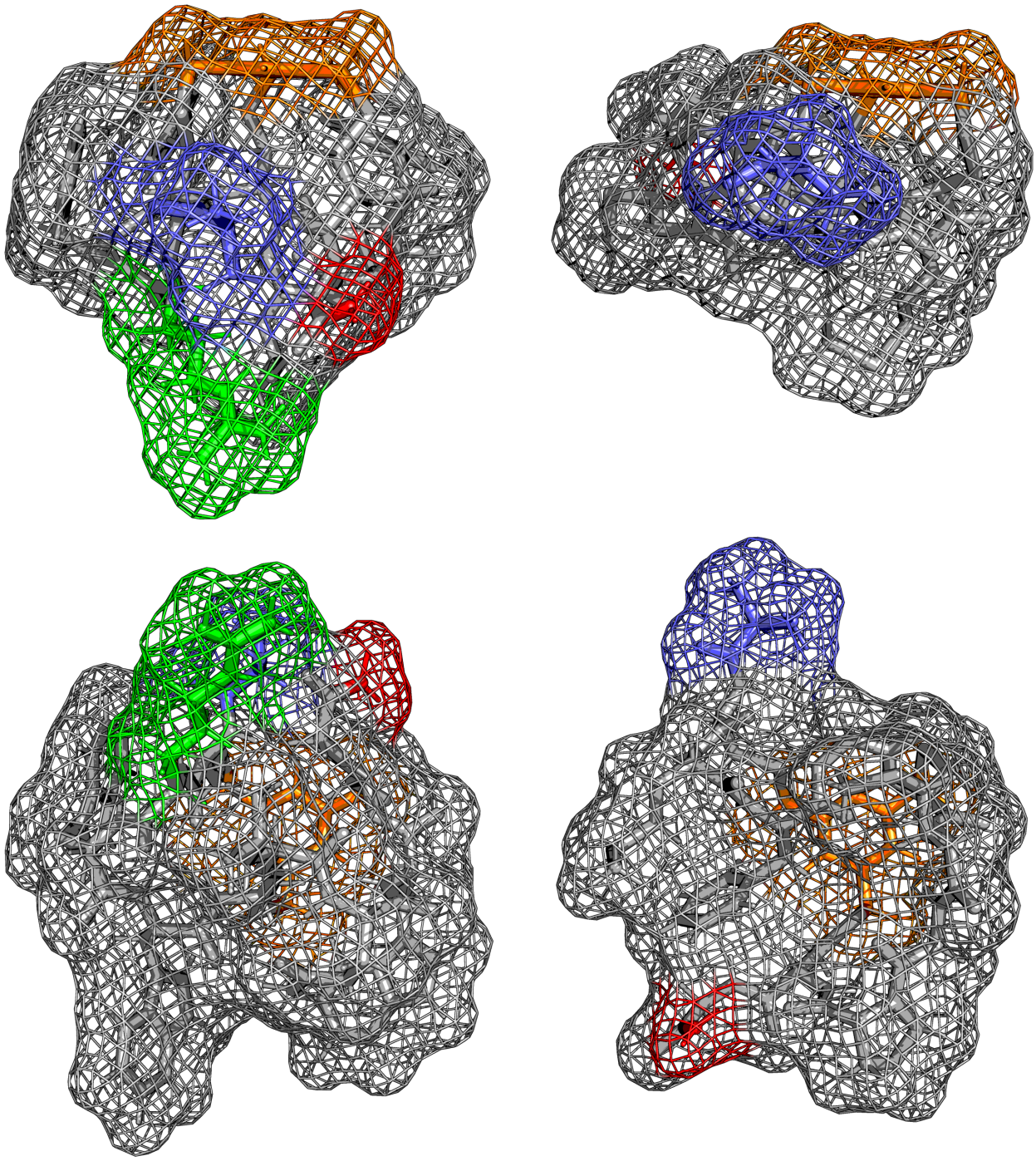

Figure S16: Lowest energy structures for Seq7 (left) and Seq8 (right), viewed from the side (top), and from opposite the linker (bottom). These sequences, in contrast to Seq4 and Seq5, were lost in the evolution. As for Seq4 and Seq5, the peptides are fairly spherical. For Seq8 there is no charged residue, likely reducing the interaction strength with the G-quadruplex. For Seq7, it is apparent in the view from below, that the positive charge and the N-terminus are very close, which does not allow for simultaneous interactions with multiple parts of the DNA structure.

S2.1 Secondary structure analysis for the bicyclic peptides

We analysed the secondary structure of the minima identified on the energy landscape, and found highly conserved features for each individual sequence, indicating a rigid backbone for these bicyclic peptides. Table S2 shows the secondary structure identified using DSSP,[1] indicating assignments found in more than 70 % of structures for each sequence.

Table S2: Observed secondary structure in the database of local minima. The key secondary structure has been highlighted: blue indicates turns, orange indicated bends, and green helices. The first loop is indicated with 1, the second loop with 2, and the cysteine residues connected to the linker are marked as C. This analysis employed CPPTRAJ[2] and DSSP.[1]

Pos	1	2	3	4	5	6	7	8	9	10	11
b-G4pep1		C	1	1	C	2	2	2	2	C	
b-G4pep2		C	1	1	1	C	2	2	2	C	
b-G4pep3		C	1	1	1	C	2	2	2	C	
Seq4		C	1	1	1	C	2	2	2	C	
Seq5		C	1	1	1	C	2	2	2	C	

S2.2 Radii of gyration and solvent-accessible surface area

The elongated shape of b-G4pep3 and the rigidity of of the backbone, especially for b-G4pep3, is evident from the distribution of the radius of gyration shown in Fig. S17 and the average values for the radius of gyration (see Table S3).

Similar behaviour is seen in the solvent-accessible surface area and its distribution, as detailed in Fig. S18 and Table S4.

Table S3: Calculated average radius of gyration for the bicyclic peptides.

	Radius of gyration (Å)	Variance (Å)
b-G4pep1	5.89 ± 0.30	0.09
b-G4pep2	6.10 ± 0.24	0.06
b-G4pep3	6.59 ± 0.09	0.01
Seq4	6.21 ± 0.22	0.05
Seq5	5.97 ± 0.19	0.19
Seq7	5.86 ± 0.13	0.02
Seq8	6.07 ± 0.11	0.01

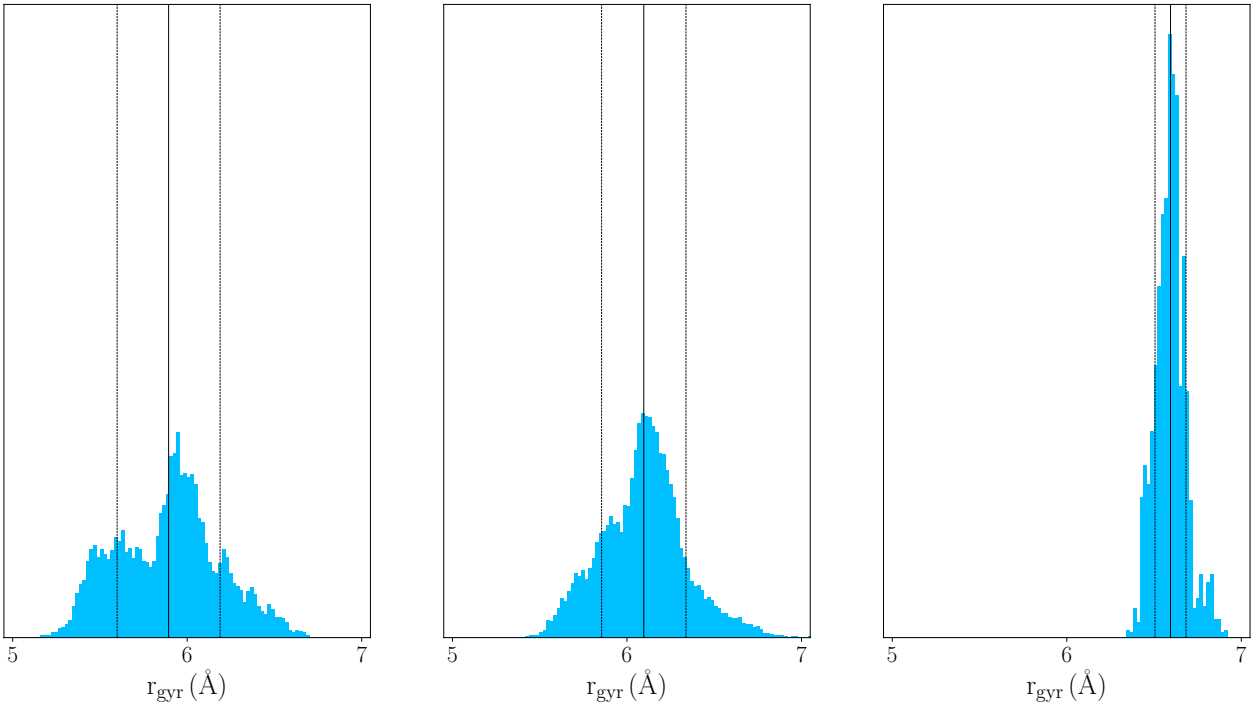

Figure S17: Histograms of the radii of gyration for all structures located on the energy landscape for b-G4pep1 (left), b-G4pep2 (middle) and b-G4pep3 (right). The average value (solid line) and standard deviation (dotted lines) are shown for each peptide. We observe smaller deviations in the radius of gyration and a larger average radius of gyration for the better binding peptide.

Table S4: Calculated average surface area of the bicyclic peptides.

	Surface area (Å^2)
b-G4pep1	1023.99 ± 47.11
b-G4pep2	1033.11 ± 42.99
b-G4pep3	1245.61 ± 29.83
Seq4	1029.99 ± 58.19
Seq5	1084.29 ± 57.66
Seq7	1065.54 ± 29.93
Seq8	1108.94 ± 36.86

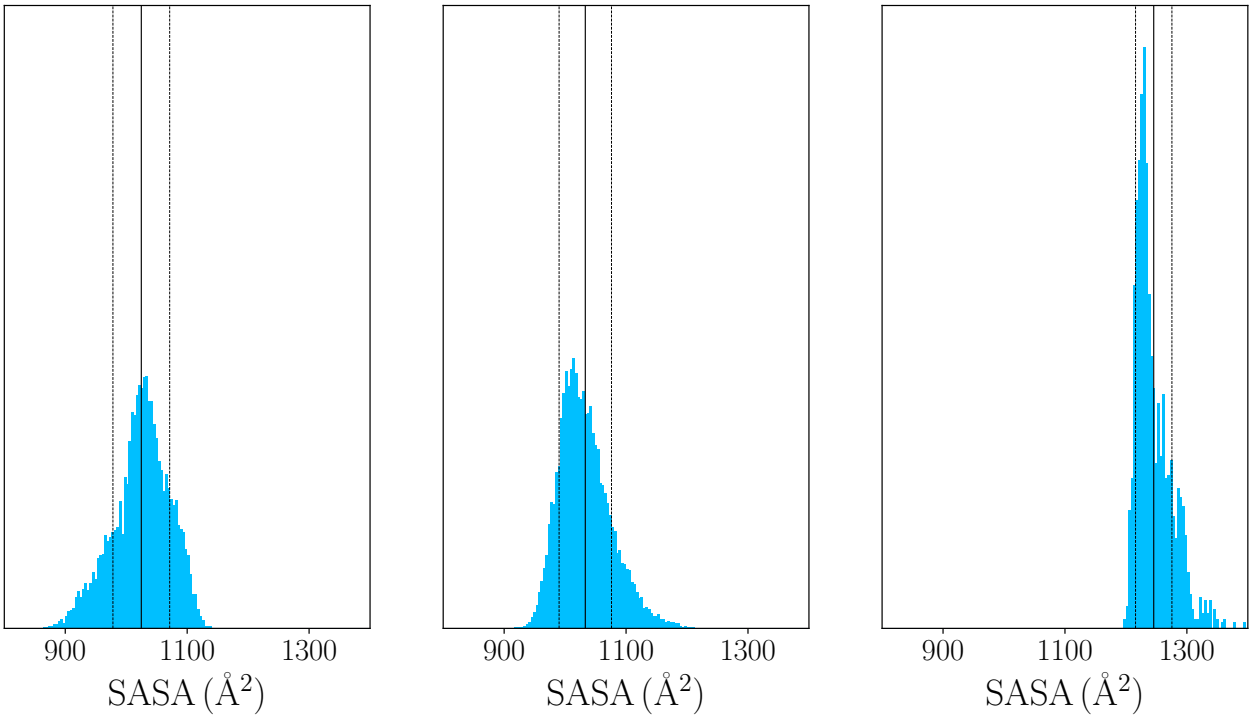

Figure S18: Histograms of the solvent-accessible surface area for the structures on the energy landscape for b-G4pep1 (left), b-G4pep2 (middle) and b-G4pep3 (right). The average value (solid line) and standard deviation (dotted lines) are shown for each peptide. We observe smaller deviations in the accessible area and a larger average area for the better binding peptides, similar to the trends observed in the radius of gyration.

S3 Supplementary data for binding simulations

In this section, we present structural measurements from the molecular dynamics simulations. We separated the analysis into different measures to identify how the individual components of the bound complex behave.

S3.1 RMS deviations in structure for the MD simualtions

In Fig. S19, the root mean square deviation of the G-quadruplex is shown with respect to the first configuration of the trajectory. All trajectories are displayed and the maximal deviation observed is around 2 Å, mainly due to motion of the nucleotides in the more flexible loop regions. No overall structural transitions are observed on the time scale of the simulations.

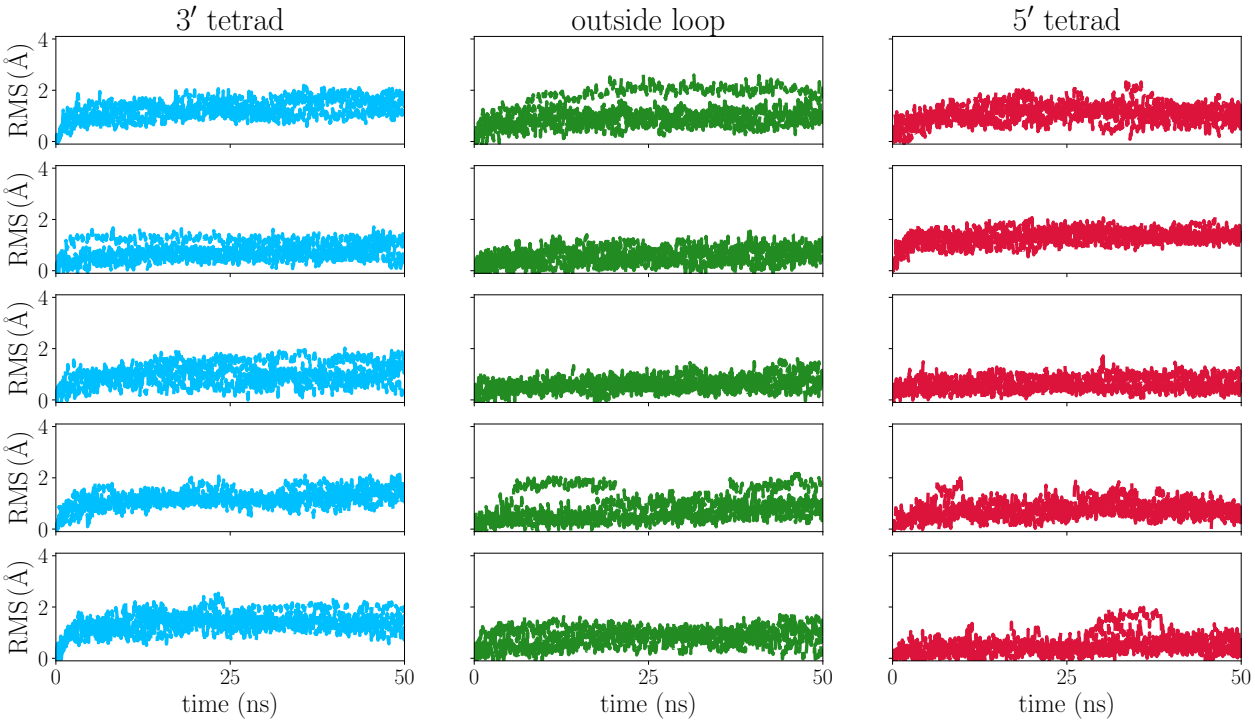

Figure S19: Root-mean square deviation for the G-quadruplex in the MD simulations relative to the starting configuration. The largest deviations observed are around 2 Å, associated with movement of the free nucleotides, and the G-quadruplex architecture itself is unchanged.

S3.2 Geometric measurements of the peptide position

In Fig. S20, S21 and S22, we analyse the behaviour of the peptide relative to the G-quadruplex. As the G-quadruplex is essentially unchanged, it is a good reference for the peptide motion, and hence the stability of the bound complex. Fig. S20 shows the distance between the geometric centre of the central tetrad and the geometric centre of the bicyclic peptide. Fig. S21 shows the distance between the peptide and the centre of nucleotides 17, 18 and 19, i.e. the central part of the AGGAG loop. Finally, Fig. S22 represents the fluctuations in the angle formed by the axis of the centres of the 3′ and 5′ tetrads, with the vector pointing from the centre of the 3′ tetrad to the geometric centre of the peptide.

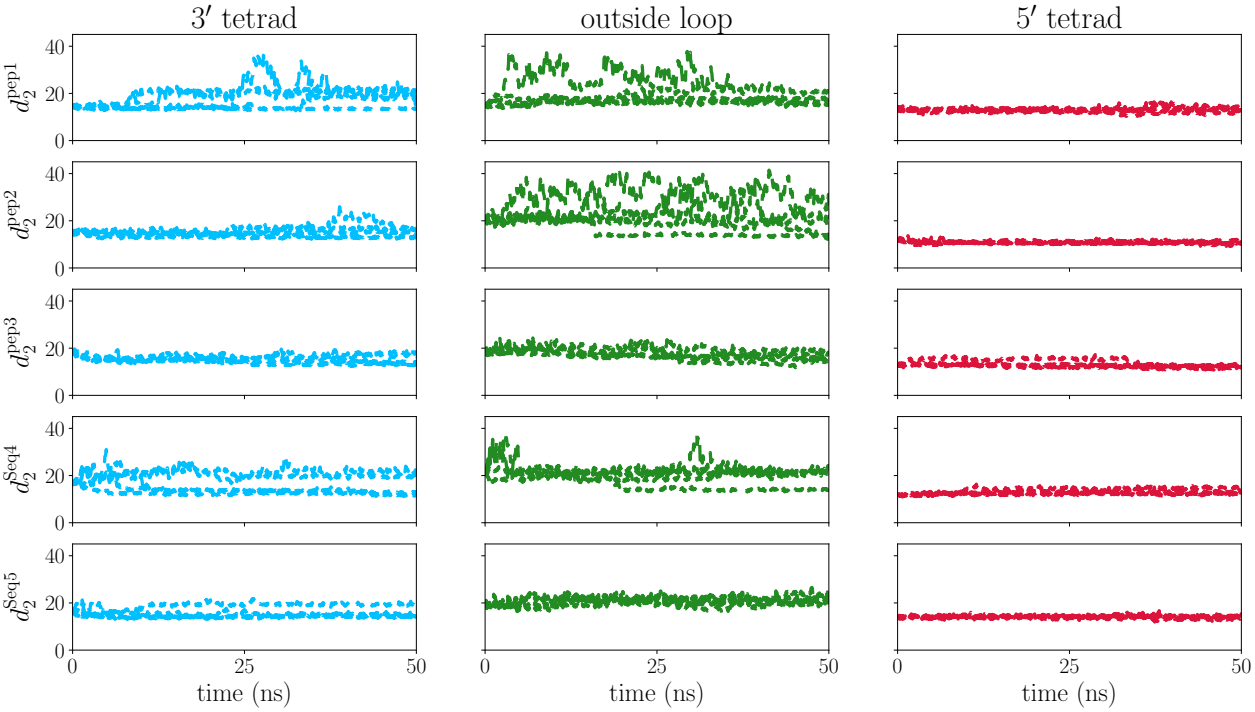

Figure S20: Distance between centre of the central tetrad and the geometric centre of the bicyclic peptide for all molecular dynamics binding simulations. While we observe large deviations for the binding outside the AGGAG loop (middle column), the deviations for the interactions with the 3′ and 5′ tetrads are much smaller.

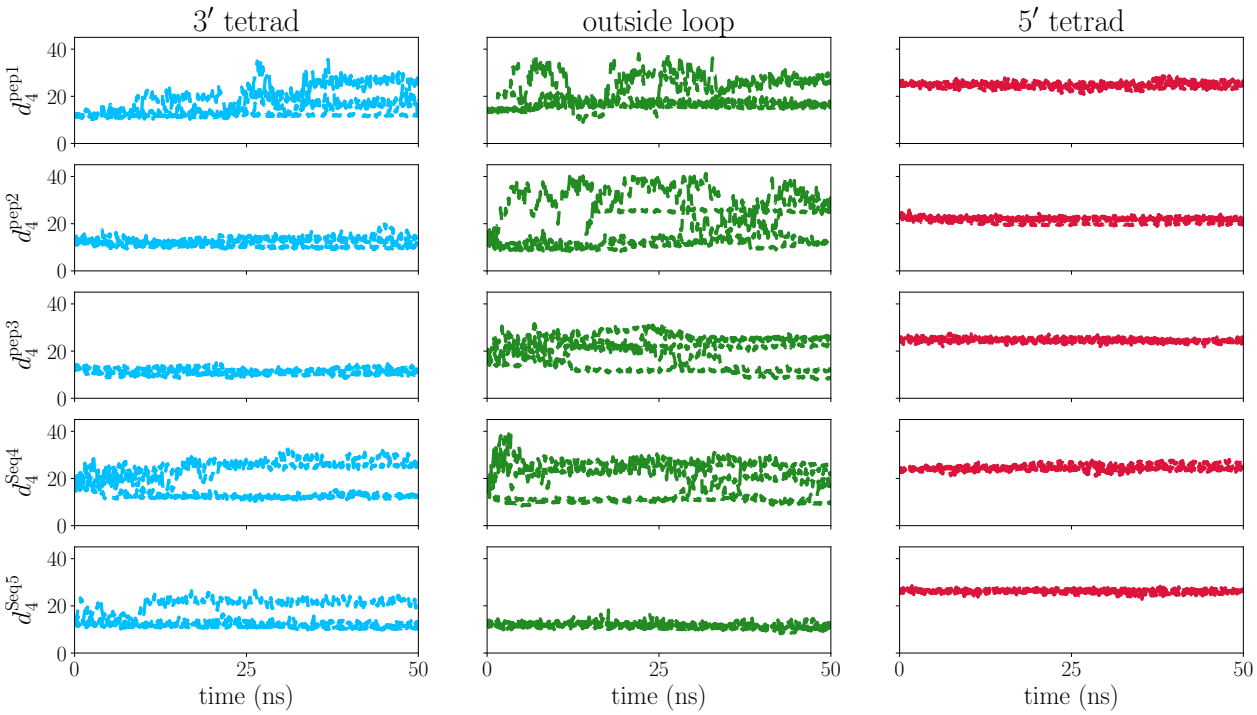

Figure S21: Distance between AGGAG loop and the geometric centre of the bicyclic peptide for all molecular dynamics binding simulations.

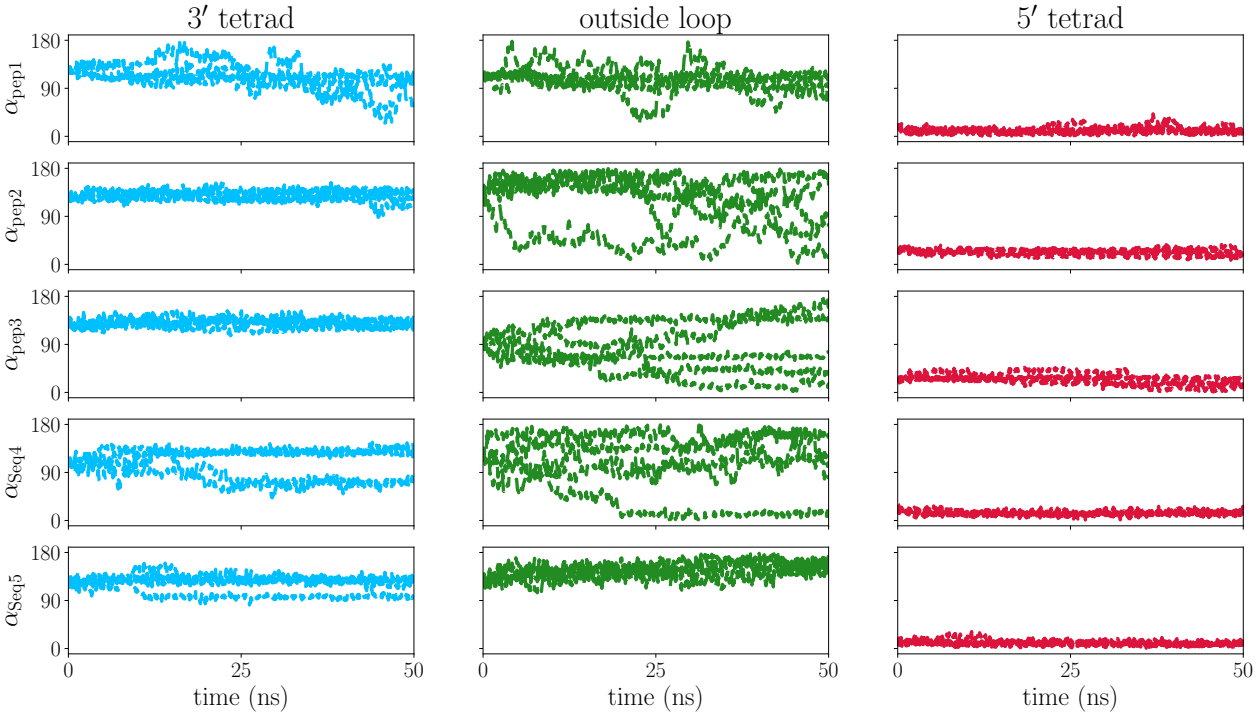

Figure S22: Angle between tetrad axis and the vector from the centre of the G-quadruplex to the bicyclic peptide.

S4 Experimental methods

S4.1 General experimental

Nuclease-free water (Millipore Milli-Q) was used for buffer/sample preparation, and other buffer components were obtained from Invitrogen, Ambion or Sigma-Aldrich at molecular biology grade, unless otherwise indicated. Primers and oligonucleotides (inc. fluorophore/biotin labelled) were obtained from Biomers unless otherwise stated.

DNA concentrations were quantified with a Thermo Scientific NanoDrop One. Agarose gel electrophoresis (0.7–2.0 wt/v%, depending on application) was conducted with Thermofisher TopVision agarose dissolved in TAE buffer, pH 7.0 (Gibco 15558042). DNA bands were stained with GelRed and visualised under UV using a Syngene Chemi XRQ Gbox. PCR amplification and incubation steps were carried out with a Peqlab peqSTAR thermocycler. qPCR were performed using a Bio-Rad CFX96 Touch Real-Time PCR Detection System. PCR products and Illumina library preparation steps were visualised and analysed on an Agilent 2200 Tapestation, using D1000 or High Sensitivity D1000 tapes. Sanger sequencing reads were obtained from Source Bioscience.

Gel extraction and PCR purification were performed using kits supplied from Zymo (Zymoclean and Clean and Concentrator) or Thermo Scientific (GeneJET), or with AMPure XP beads (Beckman Coulter) according to the manufacturer's instructions. Plasmid preparation was performed using kits from Zymo (Zyppy miniprep) or Thermo Scientific (GeneJET miniprep), and Qiagen (Endofree Plasmid Maxiprep) or Macherey-Nagel (NucleoBond PC500 maxiprep).

S4.2 Bacterial culture

LB broth (Lennox), 2-YT and SOC media were supplied from Invitrogen and used according to manufacturer's recommendations. Media sterilisation was performed with either a Enbio MicroJet microwave autoclave or a Dixons Vario 2228 autoclave. Antibiotic-selective plates

(2YT-CAM) were prepared by autoclaving media and agar (Bacto Agar, BD Biosciences 214010, 15 g/L) or LB (Lennox) agar (Invitrogen, according to manufacturer's instructions) in water. Once cooled, antibiotic was added as 1000X stock solution (chloramphenicol: 30 mg/mL in EtOH), and then poured into Nunc petri dishes (Thermo Scientific, 10 or 15 cm diameter). *E. coli* glycerol stocks for plasmid storage were prepared by adding sterile glycerol (50 v/v % in H_2O, 2X) to bacterial culture grown overnight, before freezing in liquid nitrogen.

General plasmid transformation utilised Zymo Mix & Go! chemically competent *E. coli* (strains: DH5α or TG1) according to the manufacturers' instructions.

S4.3 Synthesis of bicyclic peptides

All solvents and reagents were purified by standard procedures[3] or used as supplied from Sigma-Aldrich unless otherwise stated. Reactions were monitored with liquid chromatography-mass spectrometry (LC-MS) on a Bruker amaZon X Ion Trap MS connected to a Thermo Scientific Dionex UltiMate 3000 UHPLC with a Phenomenex Kinetex C18 column (50 × 2.1 mm, 2.6 μm) and gradient elution with MeCN in water both containing 0.1 v/v% formic acid at 1 mL/min (0.5 v/v%; 3 min, 0.5–95 v/v%; 3–6 min), monitoring with either 220 or 260 nm UV absorbance. LC-MS data were analysed using Bruker Compass DataAnalysis v.4.2. Solvents were removed under reduced pressure using a Genevac EZ-2 Elite, and lyophilisation was performed using a ScanVac CoolSafe freeze dryer. High performance liquid chromatography (HPLC) was carried out on an Interchim Puriflash prep HPLC-MS, using a Varian Pursuit C18, 5 μ column (250 × 21.2 mm) and a gradient elution with water/MeCN containing 0.1 vol.% TFA at a flow rate of 15 mL/min. High resolution mass spectrometry (HRMS) was conducted on a Waters Xevo G2-S QTof or Thermo-Finnigan Orbitrap Classic.

Linear peptides were either custom-synthesised by Genscript at >90 % purity and purified further in house by HPLC if required for biophysics, or synthesised by solid phase peptide synthesis (SPPS) carried out on a CEM Liberty Blue automated microwave peptide synthe-

siser, with a rink amide resin (Novabiochem, 100–200 mesh, loading capacity 0.58 $mmolg^{-1}$) on a 0.1 mmol scale with DMF as solvent.

Resin-immobilised peptide was then suspended in a TFA cocktail (TFA/EDT/TIPSH/Thioanisole/H_2O, 90/2.5/2.5/2.5/2.5 v/v%, 10 mL) and stirred slowly for 2–3 h. TFA and other volatile components were then removed as much as possible under reduced pressure. The peptides were precipitated and washed with cold diethyl ether (–20 °C, ~20 mL), before collecting the solid and lyophilising from 1:1 MeCN/H_2O + 0.1 v/v% TFA to yield a white solid (~100–120 mg, ~75–80 % crude).

Identity of (crude) linear peptides were first validated by LC-MS and used without further purification. Linear peptide (~30 mg) was dissolved in reaction buffer (20 mM NH_4HCO_3, 5 mM EDTA, pH = 8.0 adj. with NaOH, 12 mL) and MeCN (4 mL). TBMB (50 mM in MeCN, 250 μL) was then added, and the reaction stirred at room temperature for ~1 h, monitoring with LC-MS. Volume was decreased under reduced pressure, mixture was filtered if necessary and product purified by HPLC (5–45 % MeCN + 0.1 v/v% TFA in water + 0.1 v/v% TFA over 25 min, eluting at 13–16 min) to yield the bicyclic peptide as a white powder (10–15 mg, ~5–10 μmol, ~40 %).

S4.4 Preparation of bicyclic peptide phage display libraries

Protocols previously described by Rentero-Rebollo and Heinis[4] to produce 3×3 and 4×4 bicyclic peptide phage libraries were followed essentially verbatim. Primers were purchased from Biomers, restriction enzymes from New England Biolabs and electrocompetent cells from Lucigen. The vectors 'fdg3p0ss21' and 'fd0D1D2' were kindly provided by Prof. Christian Heinis (LPPT group, EPFL Lausanne), with permission from Prof. F.X. Schmid.

S4.5 Selection for G4 ligands

Streptavidin-coated magnetic beads were obtained from Promega (MagneSphere). Neutravidin-coated magnetic beads were obtained from GE Life Sciences (Sera-Mag SpeedBeads). gDNA competitor was salmon sperm DNA from Invitrogen (15632011). Annealing steps were carried out as follows: 95 °C; 10 min, 4 °C; 30 min. Incubation steps were conducted on a slowly rotating wheel (20 rpm). Phage titers were calculated by creating serial dilutions of phage (20 μL) and infecting TG1 *E. coli* grown to an OD_{600} ~0.4 (180 μL). These can then be spread onto 2YT-CAM plates and incubated overnight at 37 °C.

Buffers

Annealing buffer: 50 mM Tris-Cl, 100 mM KCl, pH = 7.2

Binding buffer: 10 mM Tris-Cl, 150 mM NaCl, 10mM $MgCl_2$, 1 mM $CaCl_2$, 100 mM KCl, pH = 7.4 (adj. with HCl)

Blocking buffer: Binding buffer + 0.3 v/v% Tween-20, 3 w/v% BSA

Washing buffer: Binding buffer + 0.1 v/v% Tween-20

Elution buffer: 50 mM glycine + 0.1 w/v% BSA, pH = 2.2 (adj. with HCl)

Neutralisation buffer: 1 M Tris-Cl, pH 8.0

G4 targets

Btn-hTelo: 5'–**Biotin**-GGG TTA GGG TTA GGG TTA GGG–3'

Btn-ckit-1: 5'–**Biotin**- AGG GAG GGC GCT GGG AGG AGG G–3'

Selection against hTelo

Btn-hTelo was annealed in the binding buffer (1 μM). Washed streptavidin beads (50 μL) were resuspended in the same volume of binding buffer, and annealed Btn-hTelo (500 μL) added. Two extra samples containing only beads and binding buffer were also prepared, and

all three incubated for 10 min. Unbound oligonucleotide was washed with binding buffer (500 μL $\times$3), and beads were resuspended in binding buffer (300 μL) and blocking buffer (150 μL), incubating for 30 min. At the same time, the bicyclic peptide phage library (3 ml) was incubated with blocking buffer (1.5 mL) for 30 min, and then incubated with the previously blocked streptavidin beads (450 μL) for 45 min to remove streptavidin binders. After removing these beads, the phage library was split into two 2.4 mL aliquots, and beads with and without immobilised target were each added to one aliquot, incubating for 1 h.

Beads were then collected and washed with washing buffer (500 μL $\times$6) and then binding buffer (500 μL $\times$2), exchanging tubes every 2–3 washes, before finally resuspending in elution buffer (100 μL). After 10 min, supernatant was transferred into neutralisation buffer (75 μL). The phage were then used to reinfect TG1 cells grown to OD_{600} ~0.4 (25 mL), and incubated at 37 °C for 90 min. The cells were then pelleted and spread on 2YT-CAM plates, and incubated overnight at 37 °C. If desired, aliquots of phage collected during washing steps can also be plated. Colonies were harvested with ~3 mL 2YT per plate; glycerol was added to ~15 v/v% for storage at –80 °C. Aliquots (~0.5 mL) were used to produce phage to commence the next round of selection, or processed for sequencing (see section S4.6)

Selection against ckit-1 with gDNA competition

The bicyclic peptide phage library (1X = 1.5 mL) was counterselected by addition of blocking buffer (0.75 mL) and salmon sperm DNA (gDNA competitor, 25 μL, 10 mg/mL) or hTelo (125 μL, annealed in annealing buffer at 100 μM). The phages were then incubated at 4 °C for 45 min. Annealed Btn-ckit-1 was then added (25 μL, 10 μM) to a final concentration of 100 nM, and the mixture incubated further at room temperature for 30 min. Streptavidin (round 1 and 3) or neutravidin (round 2) beads (50 μL or 5 μL respectively, washed with binding buffer) were then added and subsequently incubated for 5–10 min. Beads were then collected and washed, and phages eluted for TG1 reinfection or sequencing as described above.

S4.6 Next generation sequencing and analysis

Primers

Seq_fo: 5'–AGT TGT TCC TTT CTA TGC GGC CC–3'

Seq_rev: 5'–CGT TAG TAA ATG AAC CTT CTA TAT GG–3'

Amplifying inserts for sequencing

Plasmids were extracted from aliquots of phage libraries contained within bacterial cultures (~0.5 mL), and the insert was amplified by PCR (minimum cycles to prevent bias). Plasmids (500 ng), Seq_fo (500 nM, final conc.), Seq_rev (500 nM, final conc.), dNTP mix (each 200 μM, final conc.) and Phusion HS II HF (16 units) were mixed with Phusion buffer to a final volume of 50 μL. 50 μL aliquots were incubated in a thermocycler (95 °C; 2 min, 12 cycles of 98 °C; 20 s, 58 °C; 20 s, 72 °C, 60 s and 72 °C; 7 min). Product was purified by gel electrophoresis (1% agarose, 100 V, TAE buffer).

Library preparation, sequencing and initial processing

Next-generation sequencing was carried out on a MiSeq (Illumina), using single-end, 150-cycle kits, according to the manufacturer's instructions. Standard Illumina library preparation was carried out using the NEBNext Ultra II DNA Library Prep Kit for Illumina (New England Biolabs, E7645) with TruSeq Adapter Indexes (Illumina) following manufacturers' instructions. Libraries were quantified by qPCR using a KAPA Library Quantification Kit (Illumina) (Roche KK4824), PhiX Control v.3 (Illumina 15017397) was added as a complexity spike-in (30%).

Raw reads were then trimmed to remove adapter sequences and low quality reads using `fastx_clipper` and `fastx_quality_filter` from `http://hannonlab.cshl.edu/fastx_toolkit/index.html`. Trimmed reads were split by inline barcodes with `fastx_barcode_splitter`. Reads were then aligned against the reference sequence (AGCGTGT$(NNN)_{3/4}$TGC$(NNN)_{3/4}$

TGTGGC) using a short reference global aligner (`http://github.com/dariober/bioinformaticscafe/tree/master/eclipse/ShortRefGlobalAligner`, written by Dr Dario Beraldi). Aligned sequences were then analysed with home-made R scripts.

Summary of downstream analyses

DNA sequence plots calculated the proportion of each base (A, C, G, T or Deletion) at each aligned position. DNA sequences were translated using standard *E. coli* codons, except for TAG which was translated as Gln (TG1 strain). Amino acid distributions were calculated by counting all amino acids in the bicyclic peptide variable regions, and evaluating as percentages of the total. Library diversity was calculated using $\frac{\text{no. of unique peptides}}{\text{total no. of peptides}}$. Mutants were counted by detecting all amino acid deletions ('`---`' in base sequence) and any frameshifts ('`NN-`', '`N-N`' or '`-NN`'). SeqLogos were plotted using WebLogo v.2.8.2[5] (`https://weblogo.berkeley.edu/logo.cgi`), using the 'Frequency plot' setting, and data was plotted by multiplying each sequence by its proportion in 10,000 (e.g. a peptide sequence with 1 % proportion would be repeated 100 times). Amino acid enrichments were calculated by first calculating the proportion of each amino acid in each variable position, and then dividing the proportions after selection by the proportions before selection ($P_{\text{after}}/P_{\text{before}}$).

S4.7 G4 biophysics

For G4 biophysics, peptides (>95 % pure by UHPLC) were dissolved in water to 5 mM. Annealing G4 structures was performed as follows: heating to 95°C for 10 min and then held at 4 °C for 1 h. 96-well plates used were Bio-Rad Hard-Shell PCR plates; thin walled, white, skirted, low profile (HSP9655).

Labelled oligonucleotides

FRET_ckit-1: 5'–**FAM**-GGG AGG GCG CTG GGA GGA GGG-**TAMRA**–3'

FRET_hTelo: 5'–**FAM**-GGG TTA GGG TTA GGG TTA GGG-**TAMRA**–3'

FRET_c-Myc: 5'–**FAM**-TGA GGG TGG GTA GGG TGG GTA A-**TAMRA**–3'

FRET_dsDNA: 5'–**FAM**-TAT AGC TAT A-**HEG**-TAT AGC TAT A-**TAMRA**–3'

5'Cy5_ckit-1: 5'–**Cy5**-AGG GAG GGC GCT GGG AGG AGG G–3'

5'Cy5_hTelo: 5'–**Cy5**-AGG GTT AGG GTT AGG GTT AGG GT–3'

5'Cy5_dsDNA: 5'–**Cy5**-CAA TCG GAT CGA ATT CGA TCC GAT TG–3'

dsDNA competitor: 5'–CAA TCG GAT CGA ATT CGA TCC GAT TG–3'

ssDNA competitor: 5'–AGC GAT CTA TAG CAT GAC GT–3'

G4 competitor (ckit-1): 5'–GGG AGG GCG CTG GGA GGA GGG–3'

Buffers

FRET buffer: 60 mM potassium cacodylate, $(CH_3)_2AsO_2K$, pH = 7.4

FQ buffer: 50 mM Tris-HCl, 150 mM KCl, 0.5 w/v% CHAPS,
0.05 v/v% Triton X-100, pH 7.2

FRET melting

FRET-labelled oligonucleotides were diluted into FRET buffer at 400 nM and annealed. Dilution series were then prepared with initial ligand concentration as 100 μM in water. In a 96-well plate, subsequent serial dilutions were made by adding 50 μL of water to the same volume of ligand solution, resulting in a total of 8 or 12 concentrations including a no-ligand control of 0–100 μM ligand. 400 nM oligonucleotide solution (50 μL) was then added to each well; final conc. = 200 nM. Wells were then sealed with an adhesive transparent cover and placed on an orbital plate shaker for gentle agitation at room temperature for 1 h. Measurements were made either on a Bio-Rad CFX96 Touch Real-Time PCR Detection System, ramping from 25–95 °C at 0.5 °C min^{-1}, recording restoration of FAM signal. Melting temperatures were determined by maxima of the first derivative of RFU against

time, and ΔT_m was determined by baseline correction of melting temperatures against no-ligand control. Curve fitting utilised a one-site binding model (GraphPad Prism v.7), and variance was reported at standard error of mean.

FRET melting competition assays

dsDNA, ssDNA and G4 competitor were annealed at 40 μM in FRET buffer and annealed. FRET melting competition assays were conducted by adding annealed competitors (20 μL) at 10, 50 and 100 mol. eq. to annealed FRET oligos (20 μL, final conc. = 100 nM) and ligand (40 μL, 2X). Wells were sealed, the plate was incubated for 1 h and measurements were conducted as described in section S4.7.

Fluorescence quench equilibrium-binding assay

Protocol adapted from Le et al.[6]

Cy5 labelled oligonucleotides were diluted into assay buffer (5 mL, 50 mM Tris-HCl, pH 7.2, 150 mM KCl, 0.5 w/v% CHAPS, 0.05 v/v% Triton X-100) for 20 nM oligonucleotide solutions and annealed. Dilution series were then prepared with initial ligand concentration as 100 μM in water. Subsequent serial dilutions were made by adding 50 μL of water to the same volume of ligand solution, resulting in a total of 8 or 12 concentrations including a no-ligand control. 50 μL per solution was then transferred to a 96-well plate. 20 nM oligonucleotide solution (50 μL) was then added to each well; final conc. = 10 nM. Wells were then sealed with an adhesive foil cover and placed on an orbital plate shaker for gentle agitation at room temperature for 1 h. End-point fluorescence of each well was then measured on fluorescence plate reader (BMG PHERAstar Plus). Differences in RFU were converted to absolute values relative to the no-ligand control, and the range of these absolute values were used to normalise them to % bound. Curve fitting utilised a one-site binding model (GraphPad Prism v.7), and variance was reported at standard error of mean.

S4.8 Circular dichroism spectroscopy

Circular dichroism spectra were recorded on an Applied Photophysics Chirascan circular dichroism spectropolarimeter using a 1 mm path length quartz cuvette. Measurements were performed on bicyclic peptides (50 μM in H_2O) at 293 K from 190–330 nm using a 1 s response time, 1 nm pitch and 1 nm bandwidth. The recorded spectra represent a smoothed average of three scans, zero-corrected at 330 nm (molar ellipticity θ is quoted at 10^4 deg cm^2 dmol^{-1}), with solvent subtraction.

S5 Methods – Energy landscape explorations

S5.1 Force fields and linker model

For the bicyclic peptides, we used the properly symmetrised[7,8] ff14SB force field[9] in combination with a Generalised Born implicit solvent model (igb = 2)[10–12] and the Debye-Hückel approximation for salt (0.15 M).[13] For the linker, as it is a 1,3,5-methylated benzene, we used the standard all-atom representation types CA and HA, and CT and HC for the aromatic and tertiary carbons and hydrogens, respectively. We used CYX as the state for the linking cysteine residues, using default values for the angles and bonds on either side of the sulfur atom. The charges of the linker are zero overall. While the use of CYX would generally imply a S-S bond, the small difference in electronegativity between S and C (2.58 and 2.55 on the Pauling scale) allows the use of this residue type with a C-S bond. All sequences in Table S1 were used in this part of the study.

S5.2 Sampling procedure

Initial structures were constructed from sequence using XLEAP[14] to add the linker. After a single point optimisation using OPTIM,[15] we initiated a basin-hopping[16–18] global optimisation run in GMIN[19] from these structures consisting of 150,000 steps for each sequence. The moves used were group rotations[20,21] of the side chains, with conservation of chirality.

The 250 structures with the lowest energy were used to seed a database of stationary points for discrete path sampling[22,23] (DPS) to construct a kinetic transition network (KTN).[24,25] Within DPS, we used the doubly-nudged elastic band (DNEB) algorithm[26–29] to locate transition state candidates, which were subsequently refined accurately using hybrid eigenvector-following.[30] All minimisations use a custom L-BFGS[31,32] routine with a convergence criterion on the RMS force of 10^{-6} kcal mol^{-1} Å^{-1}. Sampling was initiated by attempting to connect all seed structures to the global minimum. Subsequent sampling focussed on unconnected components[33] and the removal of unphysical barriers[34] and kinetic

traps to converge the KTN with respect to the calculated interconversion rates.

S6 Methods – Binding simulations

S6.1 Docking procedure

Structures were docked by hand, using PyMOL.[35] We used a crystal structure for *C-kit1* avilable from the PDB databse (id: 2O3M)[36] as the template. The bicyclic peptides were then added, with the linker facing away from the G-quadruplex. The peptides were brought close enough for interactions to occur, but without introducing atom clashes. Only the five sequences highlighted in Table S1 were used in this part of the study. The *C-kit1* architecture exhibits two loops of free nucleotides, one at the 5′ tetrad, consisting of nucleotides 11 and 12 (CT), and a longer one at the 3′ tetrad, formed by nulceotides 16 to 20 (AGGAG). The AGGAG loop allows access from two sides to the 3′ tetrad, but only one of them permits easy access to the tetrad. We considered three potential binding sites for each tested sequence, namely on top of the 5′ tetrad, and the two possible ways of accessing the 3′ tetrad. The three sites are shown in Fig. S23.

S6.2 Global optimisation

The basin-hopping[16–18] global optimisation runs in GMIN[19] for the docked structures consisted of 150,000 steps for each sequence. Group rotation moves[20,21] of the peptide side chains were employed, while conserving chirality. The calculations were GPU accelerated.[37–39] The chosen force field for the peptide was ff14SB[9] and for the G-quadruplex we used ff99+bsc0.[40] As for the landscape explorations, an implicit solvent model was adopted, and no explicit ions included. The G-quadruplex is not stable in these conditions, and we therefore used rigid bodies[41–43] to constrain the tetrads and preserve the structure.

The constraints and the moves for the peptide side chains allowed us to focus on the peptide, as thge main objective of the global optimisation was to find low energy bound

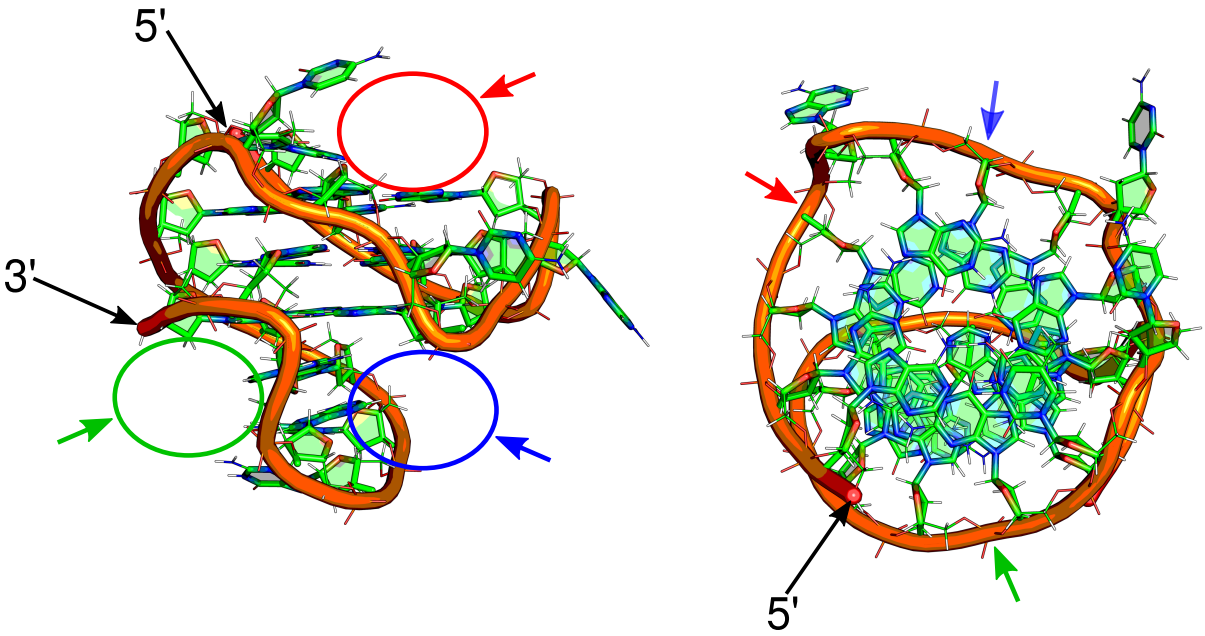

Figure S23: Representation of the potential binding sites probed in our simulations. The open 5′ tetrad side (red) is easily accessible. The two 3′ tetrad sites are smaller. Direct access to the tetrad (blue) offers a number of potential interaction sites, whereas the second way of accessing the G-quadruplex (green) at this face is more restricted.

complexes for the different binding sites and sequences, identifying whether the low energy complexes are similar across the tested sequences.

We employed four different rigidification schemes for all sequences and binding sites, resulting in 12 basin-hopping runs for every sequence. The different rigidifaction schemes allow us to identify possible errors from the rigidification, and test the stability of individual tetrads in more detail. The different schemes used are given in Table S5. The three tetrads are tetrad 1 (T1) containing nucleotides 2, 6, 10 and 13, tetrad 2 (T2) containing nucleotides 3, 7, 14 and 21, and tetrad 3 (T3) consisting of nucleotides 4, 8, 15 and 22. T1 is the 5′ tetrad, T3 the 3′ tetrad, and T2 is the central tetrad.

Schemes 1 and 2 allow us to assess the importance of relative motion of the tetrads, while for schemes 3 and 4 we gain insight into the effect of peptide binding on the exposed tetrads. For the peptide moves employed, the motion of the tetrads and the G-quadruplex as a whole will be in response to interactions with the peptide.

Table S5: Rigidification schemes applied in BH runs to avoid dissociation and unfolding of the G-quadruplex. The two-loop and the five-loop are flexible in all cases.

	Applied rigidification
Scheme 1	one rigid body containing all three tetrads
Scheme 2	three rigid bodies, one for every tetrad
Scheme 3	two rigid bodies, one for tetrad 1 and 2
Scheme 4	two rigid bodies, one for tetrad 2 and 3

S6.3 Molecular dynamics simulations

The molecular dynamics simulations serve two purposes: (a) they provide us with a more dynamical picture of the bound complexes, and (b) we use explicit solvents and ions, overcoming some limitations of the model employed in the global optimisation runs.

The simulations were carried out using the AMBER12[14] code with GPU acceleration.[37,38] The structures were solvated in a truncated octahedral box of TIP3P water molecules with a solvent buffer of at least 14 Å, on each side. The two central ions were selectively added to the G-quadruplex, along with 30 Cl^- ions and neutralising K^+ counterions. TIP3P specific ion parameters[44] were employed throughout.

The solvated system was initially minimised for 5000 steps with a 50 kcal mol^{-1} harmonic restraint on all atoms in the peptide and G-quadruplex as well as the central ions. A second minimisation was then performed without restraints. Minimisation was followed by 100 ps of heating, where the temperature was increased from zero to 300 K with harmonic restraints of 50 kcal mol^{-1} on all atoms in all amino acid residues and a time step of 2.0 fs. The temperature was regulated using a Langevin thermostat[45] employing a collision frequency of 0.2 ps^{-1}. The positional restraints were systematically reduced in three cycles of NVT dynamics each of length 50 ps at 2.0 fs steps, followed by 100 ps without constraints at 300 K. A 250 ps restrained simulation at 300 K (Langevin thermostat[45] with a collision frequency of 1.0 ps^{-1}) and a constant pressure of 1 atm was carried out to locally equilibrate the density of the solvent, followed by an otherwise identical simulation without harmonic constraints of 250 ps. This procedure was followed by a 50 ns production run in the NVT ensemble, with

5 such runs for every sequence and binding sites, resulting in 15 MD trajectories for each sequence.

References

(1) Kabsch, W.; Sander, C. Dictionary of protein secondary structure: Pattern recognition of hydrogen-bonded and geometrical features. *Biopolymers* **1983**, *22*, 2577–2637.

(2) Roe, D. R.; Cheatham III, T. E. PTRAJ and CPPTRAJ: Software for Processing and Analysis of Molecular Dynamics Trajectory Data. *J. Chem. Theory Comput.* **2013**, *7*, 3084–3095.

(3) Armarego, W. L. F.; Chai, C. L. L. *Purification of Laboratory Chemicals*, 5th ed.; Elsevier, 2003.

(4) Rentero Rebollo, I.; Heinis, C. Phage selection of bicyclic peptides. *Methods* **2013**, *60*, 46–54.

(5) Crooks, G. E.; Hon, G.; Chandonia, J.-M.; Brenner, S. E. WebLogo: a sequence logo generator. *Genome Res.* **2004**, *14*.

(6) Le, D. D.; Antonio, M. D.; Chan, L. K. M.; Balasubramanian, S. G-quadruplex ligands exhibit differential G-tetrad selectivity. *Chem. Commun.* **2015**, *51*, 8048–8050.

(7) Małolepsza, E.; Strodel, B.; Khalili, M.; Trygubenko, S.; Fejer, S. N.; Wales, D. J. Symmetrization of the AMBER and CHARMM force fields. *J. Comput. Chem.* **2010**, *31*, 1402–1409.

(8) Małolepsza, E.; Strodel, B.; Khalili, M.; Trygubenko, S.; Fejer, S. N.; Wales, D. J. Erratum to: Symmetrization of the AMBER and CHARMM force fields. *J. Comput. Chem.* **2012**, *33*, 2209.

(9) Maier, J. A.; Martinez, C.; Kasavajhala, K.; Wickstrom, L.; Hauser, K. E.; Simmerling, C. ff14SB: Improving the accuracy of protein side chain and backbone parameters from ff99SB. *J. Chem. Theory Comput.* **2015**, *11*, 3696–3713.

(10) Onufriev, A.; Bashford, D.; Case, D. A. Modification of the generalized Born model suitable for macromolecules. *J. Phys. Chem. B* **2000**, *104*, 3712–3720.

(11) Onufriev, A.; Case, D. A.; Bashford, D. Effective Born radii in the generalized Born approximation: The importance of being perfect. *J. Comput. Chem.* **2002**, *23*, 1297–1304.

(12) Onufriev, A.; Bashford, D.; Case, D. A. Exploring protein native states and large-scale conformational changes with a modified generalized born model. *Proteins* **2004**, *55*, 383–394.

(13) Srinivasan, J.; Trevathan, M. W.; Beroza, P.; Case, D. A. Application of a pairwise generalized Born model to proteins and nucleic acids: inclusion of salt effects. *Theor. Chem. Acc.)* **1999**, *101*, 426–434.

(14) `AMBER12`. Case, D.A. et al.: University of California, San Francisco, 2012.

(15) `OPTIM` - a program for optimising geometries and calculating reaction pathways. Wales, David J.: Cambridge, 2018.

(16) Li, Z.; Scheraga, H. A. Monte Carlo-minimization approach to the multiple-minima problem in protein folding. *Proc. Natl. Acad. Sci. USA* **1987**, *84*, 6611–6615.

(17) Li, Z.; Scheraga, H. A. Structure and free-energy of complex thermodynamic systems. *J. Mol. Struct.* **1988**, *48*, 333–352.

(18) Wales, D. J.; Doye, J. P. K. Global optimization by basin-hopping and the lowest energy structures of Lennard-Jones clusters containing up to 110 atoms. *J. Chem. Phys. A* **1997**, *101*, 5111–5116.

(19) `GMIN` - a program for basin-hopping global optimisation, basin-sampling, and parallel tempering. **2018**,

(20) Mochizuki, K.; Whittleston, C. S.; Somani, S.; Kusumaatmaja, H.; Wales, D. J. A conformational factorisation approach for estimating the binding free energies of macromolecules. *Phys. Chem. Chem. Phys.* **2014**, *16*, 2842–2853.

(21) Oakley, M. T.; Johnston, R. L. Energy landscapes and global optimization of self-assembling cyclic peptides. *J. Chem. Theory Comput.* **2014**, *10*, 1810–1816.

(22) Wales, D. J. Discrete path sampling. *Mol. Phys.* **2002**, *100*, 3285–3305.

(23) Wales, D. J. Some further applications of discrete path sampling to cluster isomerization. *Mol. Phys.* **2004**, *102*, 891–908.

(24) Noé, F.; Fischer, S. Transition networks for modeling the kinetics of conformational change in macromolecules. *Curr. Opin. Struc. Biol.* **2008**, *18*, 154–162.

(25) Wales, D. J. Energy landscapes: some new horizons. *Curr. Opin. Struc. Biol.* **2010**, *20*, 3–10.

(26) Henkelman, G.; Jónsson, H. A dimer method for finding saddle points on high dimensional potential surfaces using only first derivatives. *J. Chem. Phys.* **1999**, *111*, 7010–7022.

(27) Henkelman, G.; Uberuaga, B. P.; Jónsson, H. A climbing image nudged elastic band method for finding saddle points and minimum energy paths. *J. Chem. Phys.* **2000**, *113*, 9901–9904.

(28) Trygubenko, S. A.; Wales, D. J. A doubly nudged elastic band method for finding transition states. *J. Chem. Phys.* **2004**, *120*, 2082–2094.

(29) Sheppard, D.; Terrell, R.; Henkelman, G. Optimization methods for finding minimum energy paths. *J. Chem. Phys.* **2008**, *128*, 134106.

(30) Munro, L. J.; Wales, D. J. Defect migration in crystalline silicon. *Phys. Rev. B* **1999**, *59*, 3969–3980.

(31) Nocedal, J. Updating quasi-newton matrices with limited storage. *Math. Comput.* **1980**, *35*, 773.

(32) Liu, D.; Nocedal, J. On the limited memory bfgs method for large scale optimization. *Math. Prog.* **1989**, *45*, 503.

(33) Röder, K.; Wales, D. J. Energy landscapes for the aggregation of Aβ_{17-42}. *J. Am. Chem. Soc.* **2018**, *140*, 4018–4027.

(34) Strodel, B.; Whittleston, C. S.; Wales, D. J. Thermodynamics and kinetics of aggregation for the GNNQQNY peptide. *J. Am. Chem. Soc.* **2007**, *129*, 16005–16014.

(35) The PyMOL Molecular Graphics System, Version 1.6.x. Schrödinger, LLC: New York, 2013.

(36) Phan, A. T.; Kuryavyi, V.; Burge, S.; Neidle, S.; Patel, D. J. Structure of an unprecedented G-quadruplex scaffold in the human c-kit promoter. *J. Am. Chem. Soc.* **2007**, *129*, 4386–4392.

(37) Götz, A. W.; Williamson, M. J.; Xu, D.; Poole, D.; Le Grand, S.; Walker, R. C. Routine microsecond molecular dynamics simulations with AMBER on GPUs. 1. Generalized Born. *J. Chem. Theory Comput.* **2012**, *8*, 1542–1555.

(38) Salomon-Ferrer, R.; Götz, A. W.; Poole, D.; Le Grand, S.; Walker, R. C. Routine microsecond molecular dynamics simulations with AMBER on GPUs. 2. Explicit Solvent Particle Mesh Ewald. *J. Chem. Theory Comput.* **2013**, *9*, 3878–3888.

(39) Mantell, R. G.; Pitt, C. E.; Wales, D. J. GPU-accelerated exploration of biomolecular energy landscapes. *J. Chem. Theory Comput.* **2016**, *12*, 6182–6191.

(40) Pérez, A.; Marchán, I.; Svozil, D.; Sponer, J.; Cheatham, T. E.; Laughton, C. A.; Orozco, M. Refinement of the AMBER force field for nucleic acids: Improving the description of α/γ conformers. *Biophys. J.* **2007**, *92*, 3817–3829.

(41) Kusumaatmaja, H.; Whittleston, C. S.; Wales, D. J. A local rigid body framework for global optimization of biomolecules. *J. Chem. Theory Comput.* **2012**, *8*, 5159–5165.

(42) Rühle, V.; Kusumaatmaja, H.; Chakrabarti, D.; Wales, D. J. Exploring energy landscapes: Metrics, pathways, and normal-mode analysis for rigid-body molecules. *J. Chem. Theory Comput.* **2013**, *9*, 4026–4034.

(43) Joseph, J. A.; Whittleston, C. S.; Wales, D. J. Structure, thermodynamics, and folding pathways for a tryptophan zipper as a function of local rigidification. *J. Chem. Theory Comput.* **2016**, *12*, 6109–6117.

(44) Joung, I. S.; Cheatham, T. E. Determination of alkali and halide monovalent ion parameters for use in explicitly solvated biomolecular simulations. *J. Phys. Chem. B.* **2008**, *112*, 9020–9041.

(45) Loncharich, R. J.; Brooks, B. R.; Pastor, R. W. Langevin dynamics of peptides: The frictional dependence of isomerization rates of N-actylananyl-N′-methylamide. *Biopolymers* **1992**, *32*, 523–535.